**Cite this article as:** Vadalà, F., Bacigalupo, A., Lepidi, M., Gambarotta L. (2021). Free and forced wave propagation in beam lattice metamaterials with viscoelastic resonators. International Journal of Mechanical Sciences 193, id.106129.

# Free and forced wave propagation in beam lattice metamaterials with viscoelastic resonators

Francesca Vadalà[a], Andrea Bacigalupo[a], Marco Lepidi[a,*], Luigi Gambarotta[a]

[a] *DICCA - Dipartimento di Ingegneria Civile, Chimica e Ambientale, Università di Genova, Via Montallegro 1, 16145 Genova (Italy)*

**Abstract**

Beam lattice materials are characterized by a periodic microstructure realizing a geometrically regular pattern of elementary cells. The dispersion properties governing the free dynamic propagation of elastic waves can be studied by formulating parametric discrete models of the cellular microstructure and applying the Floquet-Bloch theory. Within this framework, governing the wave propagation by means of spectral design techniques and/or energy dissipation mechanisms is a major issue of theoretical and applied interest. Specifically, the wave propagation can be inhibited by purposely designing the microstructural parameters to open stop bands in the material spectrum at target center frequencies. Based on these motivations, a general dynamic formulation is presented for determining the dispersion properties of mechanical metamaterials, modeled as locally resonant beam lattices with generic coordination number. The mechanism of local resonance is realized by tuning periodic auxiliary oscillators, viscoelastically coupled with the beam lattice microstructure. As peculiar aspect, the viscoelastic coupling is derived by a mechanical formulation based on the Boltzmann superposition integral, whose kernel is approximated by a Prony series. Consequently, the free propagation of damped waves is governed by a linear homogeneous system of integro-differential equations of motion. Therefore, differential equations of motion with frequency-dependent viscoelastic coefficients are obtained by applying the in-space $\mathcal{Z}$-transform and in-time bilateral Laplace transform. The complex-valued branches characterizing the dispersion spectrum are determined and parametrically analyzed for the beam lattice characterized by quadrilateral periodic cell. The spectral branches may exceed the model dimension, due to the occurrence of pure-damping spectral components. Particularly, the spectra corresponding to Laurent series approximations of the viscoelastic coefficients are investigated and the solution admissibility and convergence for increasing order series is analyzed. The standard dynamic equations with linear viscous damping are recovered at the first-order approximation. Low-order approximations are found to underestimate the real and imaginary parts of the spectrum, as well as the low-frequency stop bandwidth. Finally, the forced response to a harmonic mono-frequent external point excitation is investigated. The metamaterial responses to non-resonant, resonant and quasi-resonant external forces are compared and discussed from a qualitative and quantitative viewpoint.

*Keywords:* Periodic materials, acoustic metamaterials, dispersion properties, viscous damping, complex band structure, band gaps.

*Corresponding author
*Email address:* marco.lepidi@unige.it (Marco Lepidi)

## 1. Introduction

Microstructured material and metamaterial science is a challenging frontier of theoretical and applied research that is currently attracting growing interest by the scientific community of solid and structural mechanicians [1–5]. Specifically, the conceptualization and development of novel materials, characterized by smart or unconventional functionalities, are continuously propelled by the recent extraordinary developments in the technological fields of super-computing, micro-engineering and high-precision manufacturing [6–8]. As valuable result of this successful research trend, a new generation of architected composites is deeply transforming and rapidly remodeling the traditional paradigms of rational design in a variety of technical multidisciplinary applications across all the classical and advanced branches of mechanics, including – among the others – extreme mechanics, nanomechanics, mechatronics, acoustics, thermomechanics, biomechanics [9–12].

Within this stimulating framework, composite materials and mechanical (or acoustic) metamaterials with periodic cellular microstructure are being purposely designed to achieve superior effective properties, outperforming the elasto-dynamic characteristics of the ingredient materials building each microstructured cell [13–15]. Significant achievements have been obtained in tailoring unusual properties or exotic performances, including for instance super lightness-to-strength ratios, strong auxeticity, synclastic bending curvatures, giant hysteresis, morphing and multi-stability, negative indexes of dynamic refraction, nonreciprocal vibration propagation, broadband sound absorption, controllable wave guiding, obstacle cloaking, low-frequency noise filtering, energy focusing or harvesting [16–25].

Focusing on the dynamic response of periodic cellular media, a major issue of mechanical interest consists in governing the wave propagation by means of spectral design techniques and/or energy dissipation mechanisms. To this purpose, the wave propagation around certain target center-frequencies can be inhibited by finely designing the microstructural parameters in order to open band gaps in the material dispersion spectrum. Basically, the design problem can be stated either as an inverse problem or as an optimization problem. According to the former approach, the linear eigenproblem governing the free wave propagation can be stated, solved and – in principle – inverted to analytically assess the microstructural parameters satisfying desired spectral requirements, like the existence, position and amplitude of a given harmonic component or certain pass or stop bands in the frequency spectrum [26–28]. Of course, solving the inverse problem may be not straightforward and – in the general case – some forms of mathematical approximations (e.g. asymptotic perturbation-based solutions) must be accepted to preserve the analytical assessment of the design variables [29, 30]. According to the latter approach, a suited objective or multi-objective function can be formulated, so that its maximization or minimization allows the numerical identification of the optimal solution in the multidimensional space of the design parameters [31–33]. Generally, a proper mathematical surrogation of the objective function may help in reducing the computational costs and accelerating the algorithmic convergence [34]. Independently of the particular approach, the existence, uniqueness and admissibility of the design solution must be discussed. In the spectral design of cellular periodic materials for low-frequency wave filtering, the extent and dimensionality of the optimal solution domain can be significantly enlarged by designing mechanical metamaterials, realized by introducing auxiliary massive oscillators, mechanically coupled to the cell microstructure. Indeed, if the oscillators are properly tuned (local resonators), their dynamic interaction with the microstructure ends up opening a band gap in the dispersion spectrum [35, 36]. It can be demonstrated that the achievable band gap is nearly centered at the oscillator frequency, with a bandwidth almost directly proportional to its mass [30, 37–39]. Accordingly, different parametric forms of spectral design tend to realize the desirable optimum of maximizing the band gap amplitude centered at the lowest center frequency by introducing heavy oscillators, weakly coupled with the microstructure [37, 40]. It may be worth remarking that the peculiar mechanism of local resonance can be virtuously exploited to achieve other desirable effects, including modal localization, transmission amplification, image lensing, wave trapping and edging [41–44].

Starting from this scientific background, formulating microstructural models of locally-resonant mechanical metamaterials is an active research field, whose development is motivated by some open investigation issues. First, a general improvement in the elastodynamic description of the linear and nonlinear dissipation mechanisms occurring in infinite periodic phononic systems has been recognized as the theoretical key point for the future advances in the energetically consistent modelization and spectral design

of mechanical metamaterials [14]. Second, a completely new class of mechanical meta-behaviours has been postulated to be developable in the next few years, by exploiting the virtuous contrast and synergy among constituent ingredient materials featured by strongly dissimilar elastic, plastic and viscous properties [15]. Based on these motivations, the paper presents a beam lattice formulation for describing the wave dynamics of an mechanical metamaterial, originated by a periodic non dissipative microstructure viscoelastically coupled with local resonators. As original aspect, the viscoelastic coupling is consistently derived by a physical-mathematical construct based on the Boltzmann superposition integral, whose kernel is approximated by a Prony series [45]. Consequently, the non-conservative wave propagation is governed by a linear homogeneous system of integro-differential equations of motion. This integral description of the viscoelastic metamaterial dissipation enriches the classic formulations of viscous damping, sometimes following the rheological Rayleigh or Maxwell models [46, 47], which can be recovered for particular parameter values and low-order approximations of the governing equations in the transformed $\mathcal{Z}$-Laplace space. According to the so-called inverse method [14], the associated non-polynomial eigenproblem is solved in the space of complex frequencies and real wavevectors. Therefore, the complex frequencies can be expressed in terms of real-valued damped frequencies and damping ratio [48–50]. This solution approach differs from the so-called direct method [14], in which the governing eigenproblem is solved in the space of real frequencies and complex wavevectors [51–56]. Specifically, the latter approach has been successfully employed in studying lossy phononic crystals [53] and periodic heterogeneous materials [54] containing viscoelastic phases. Moreover, the viscoelastic effects on the wave dispersion properties have been theoretically and experimentally investigated in mechanical metamaterials, by introducing the material losses through stress-strain relations in terms of hereditary or Duhamel integrals [55–57].

In order to characterize the free and forced propagation of damped waves in the mechanical metamaterials, a Lagrangian linear model of the periodic beam lattice microstructure, visco-elastically coupled with local resonators, is formulated (Section 2). Therefore, the dynamic problem concerning the wave propagation of damped waves is stated according to the Floquet-Bloch theory (Section 3). First, the complex dispersion spectrum characterizing the free dynamics is determined for the beam lattice with quadrilateral elementary cell, and the admissibility and convergence of increasing order approximations of the coupling relaxation functions is discussed, with reference to the exact dispersion curves (Section 4). Second, the forced response to a harmonic mono-frequent external point source is investigated in the frequency and time domain for the fundamental cases of non-resonant, resonant and quasi-resonant external force (Section 5). Finally, concluding remarks are pointed out.

## 2. Equations of motion

The periodic microstructure of mechanical metamaterials with viscoelastic resonators can be based on different cellular topologies characterized by the coordination number $n$. The centrosymmetric periodic cell of the planar triangular ($n = 6$) and quadrilateral ($n = 4$) metamaterials is geometrically featured by the characteristic size $a$ (Figure 1a). The out-of-plane depth $d$ can be assumed unitary without loss of generality. From the physical viewpoint, the cell microstructure is characterized by a central massive stiff ring with mean radius $R$. Each ring is connected with the rings of the adjacent cells by $n$ identical flexible and light ligaments with length $L = a - 2R$ and constant width $w$. According to a beam lattice formulation, the stiff rings are described as rigid bodies with mass $M_1$ and rotational inertia $J_1$, while the flexible ligaments are modeled as linear unshearable massless beams with elastic modulus $E$. The ring-ligament connections are assumed to realize perfectly rigid joints. The in-plane motion of the generic rigid ring is described by the displacement vector $\mathbf{u}$ and the rotation $\phi$, referred to the configuration node located at the ring centroid.

In order to realize the distinctive mechanism of local resonance, each ring hosts a heavy stiff disk with radius $r$, co-centered with the housing ring and embedded in a soft annular matrix of viscoelastic material. The stiff disk is mechanically modeled as a circular rigid body that plays the role of tuned oscillator (*local resonator*) with mass $M_2$ and rotational inertia $J_2$. The viscoelastic ring-resonator coupling is synthetically described by the time-dependent relaxation functions $k_d(t)$ for the relative displacement and $k_a(t)$ for the relative rotation. The in-plane motion of the generic resonator is described by the displacement vector $\mathbf{v}$ and the rotation $\theta$, referred to the configuration node located at the disk centroid (Figure 1b). Consequently,

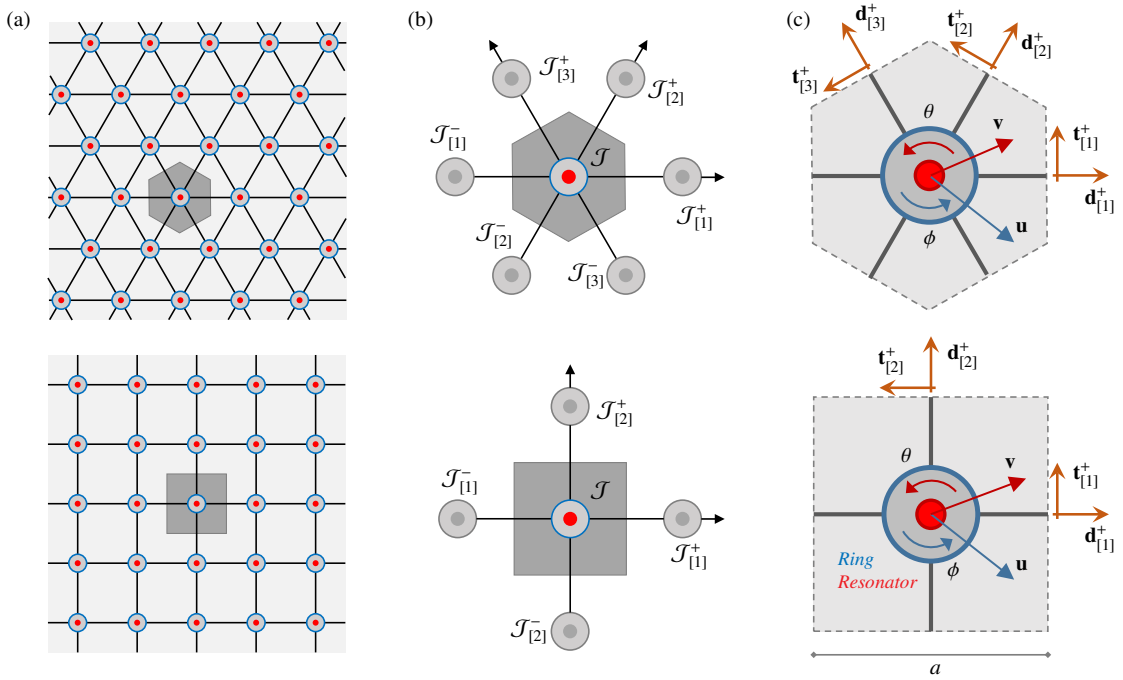


Figure 1: Beam lattice metamaterials with viscoelastic resonator: (a) cellular topologies and periodic cell, (b) coordination directions, (c) mechanical model.

the reference positions of the centroidal nodes of the ring and the disk are geometrically coincident to each other (*two-node lattice point*) in the natural configuration. The generic periodic cell is assumed externally excited by in-plane dynamic actions reducible to a time-dependent nodal force $\mathbf{f}$ and moment $g$, applied at the centroidal node of the ring. The resonator is supposed unloaded.

According to the mechanical assumptions, the integro-differential equations of motion governing the forced dynamics of the beam lattice metamaterial characterized by a generic *coordination number* $n$ (with $n=4$ and $n=6$ for the quadrilateral and triangular lattices, respectively) read

$$
\begin{aligned}
&M_1\ddot{\mathbf{u}}_{\mathcal{J}}+\int_{-\infty}^{t}k_d(t-\tau)\tfrac{d}{d\tau}\left(\mathbf{u}_{\mathcal{J}}-\mathbf{v}_{\mathcal{J}}\right)\mathrm{d}\tau+\textstyle\sum_{\mathcal{P}^+_{[\mathrm{j}]}}\mathbf{r}^+_{\mathcal{J}_{[\mathrm{j}]}}+\sum_{\mathcal{P}^-_{[\mathrm{j}]}}\mathbf{r}^-_{\mathcal{J}_{[\mathrm{j}]}}=\mathbf{f}_{\mathcal{J}},\\
&J_1\ddot{\phi}_{\mathcal{J}}+\int_{-\infty}^{t}k_a(t-\tau)\tfrac{d}{d\tau}\left(\phi_{\mathcal{J}}-\theta_{\mathcal{J}}\right)\mathrm{d}\tau+\textstyle\sum_{\mathcal{P}^+_{[\mathrm{j}]}}c^+_{\mathcal{J}_{[\mathrm{j}]}}+\sum_{\mathcal{P}^-_{[\mathrm{j}]}}c^-_{\mathcal{J}_{[\mathrm{j}]}}=g_{\mathcal{J}},\\
&M_2\ddot{\mathbf{v}}_{\mathcal{J}}+\int_{-\infty}^{t}k_d(t-\tau)\tfrac{d}{d\tau}\left(\mathbf{v}_{\mathcal{J}}-\mathbf{u}_{\mathcal{J}}\right)\mathrm{d}\tau=\mathbf{0},\\
&J_2\ddot{\theta}_{\mathcal{J}}+\int_{-\infty}^{t}k_a(t-\tau)\tfrac{d}{d\tau}\left(\theta_{\mathcal{J}}-\phi_{\mathcal{J}}\right)\mathrm{d}\tau=0,
\end{aligned}
\tag{1}
$$

where $\mathcal{J}=(i_1,...,i_{n/2})$ is the set of coordination directions of the lattice, which identifies a particular lattice node when all the $i$-indices are specified. The inter-cellular internal forces exerted on the $\mathcal{J}$-th node are

$$
\begin{aligned}
&\mathbf{r}^+_{\mathcal{J}_{[\mathrm{j}]}}=\mathbf{K}^+_{[\mathrm{j}]}(\mathbf{u}_{\mathcal{J}_{[\mathrm{j}]}}-\mathbf{u}_{\mathcal{J}^+_{[\mathrm{j}]}})+\mathbf{k}^+_{[\mathrm{j}]}(\phi_{\mathcal{J}_{[\mathrm{j}]}}+\phi_{\mathcal{J}^+_{[\mathrm{j}]}}),\\
&\mathbf{r}^-_{\mathcal{J}_{[\mathrm{j}]}}=\mathbf{K}^-_{[\mathrm{j}]}(\mathbf{u}_{\mathcal{J}_{[\mathrm{j}]}}-\mathbf{u}_{\mathcal{J}^-_{[\mathrm{j}]}})+\mathbf{k}^-_{[\mathrm{j}]}(\phi_{\mathcal{J}_{[\mathrm{j}]}}+\phi_{\mathcal{J}^-_{[\mathrm{j}]}}),\\
&c^+_{\mathcal{J}_{[\mathrm{j}]}}=\mathbf{k}^+_{[\mathrm{j}]}\cdot(\mathbf{u}_{\mathcal{J}_{[\mathrm{j}]}}-\mathbf{u}_{\mathcal{J}^+_{[\mathrm{j}]}})+K_a(\phi_{\mathcal{J}_{[\mathrm{j}]}}+\phi_{\mathcal{J}^+_{[\mathrm{j}]}})+K_\ell(\phi_{\mathcal{J}_{[\mathrm{j}]}}-\phi_{\mathcal{J}^+_{[\mathrm{j}]}}),\\
&c^-_{\mathcal{J}_{[\mathrm{j}]}}=\mathbf{k}^-_{[\mathrm{j}]}\cdot(\mathbf{u}_{\mathcal{J}_{[\mathrm{j}]}}-\mathbf{u}_{\mathcal{J}^-_{[\mathrm{j}]}})+K_a(\phi_{\mathcal{J}_{[\mathrm{j}]}}+\phi_{\mathcal{J}^-_{[\mathrm{j}]}})+K_\ell(\phi_{\mathcal{J}_{[\mathrm{j}]}}-\phi_{\mathcal{J}^-_{[\mathrm{j}]}}),
\end{aligned}
\tag{2}
$$

where the auxiliary set $\mathcal{J}_{[\mathrm{j}]}=(i_1,...,i_{\mathrm{j}},...,i_{n/2})$ allows to select the $i$-th lattice node along the coordination direction $i_{\mathrm{j}}$ specified by the j-subscript, while $\mathcal{J}^{\pm}_{[\mathrm{j}]}=(i_1,...,i_{\mathrm{j}}\pm1,...,i_{n/2})$ allows to select the $(i\pm1)$-th lattice nodes by incrementing or decrementing the index $i_{\mathrm{j}}$ along the coordination direction specified by the j-subscript. The sets $\mathcal{P}^+_{[\mathrm{j}]}$ or $\mathcal{P}^-_{[\mathrm{j}]}$ collect the $j$-values identifying the positive ($j=1,...,n/2$) and negative ($j=-1,...,-n/2$) directions, respectively.

In synthesis, the linear system of ordinary-differential coupled equations (1) governs the forced damped oscillations at the $\mathcal{J}$-th node of the beam lattice. The extensional-bending coupling between adjacent rings is specified by the beam stiffness coefficients $\mathbf{K}^{\pm}_{[\mathrm{j}]}$, $\mathbf{k}^{\pm}_{[\mathrm{j}]}$, $K_a$, $K_\ell$. The *local* nature of the ring-resonator coupling is expressed by the $\mathcal{J}^{\pm}_{[\mathrm{j}]}$-independence of the equations governing the resonator dynamics. Considering that no inherent structural damping is introduced, the dynamic equations governing the non-dissipative beam lattice metamaterial are recovered if the relaxation functions are assumed time-independent [53].

Denoting by $\omega_r$ and $L_r$ a pair of known dimensional quantities, suited to serve as reference frequency and length of the metamaterial, respectively, a convenient nondimensional form (valid for all the subscripts) of the independent and dependent variables can be introduced

$$\tilde{t}=\omega_r t, \qquad \tilde{\tau}=\omega_r \tau, \qquad \tilde{\mathbf{u}}=\frac{\mathbf{u}}{L_r}, \qquad \tilde{\mathbf{v}}=\frac{\mathbf{v}}{L_r}, \qquad \tilde{\mathbf{f}}=\frac{\mathbf{f}}{\omega_r^2 M_1 L_r}, \qquad \tilde{g}=\frac{g}{\omega_r^2 M_1 L_r^2}, \tag{3}$$

and a minimal sufficient set of nondimensional mechanical parameter can be defined

$$\begin{gathered}\varrho^2=\frac{M_2}{M_1}, \qquad \chi_1^2=\frac{J_1}{M_1 L_r^2}=\frac{R^2}{L_r^2}, \qquad \chi_2^2=\frac{J_2}{M_2 L_r^2}=\frac{r^2}{2L_r^2}, \qquad \eta^2=\frac{Ea}{\omega_r^2 M_1}, \\ \kappa_d=\frac{k_d}{Ea}, \qquad \kappa_a=\frac{k_a}{EaL_r^2}, \qquad \alpha=\frac{a}{L_r}, \qquad \delta=\frac{d}{a}, \qquad \mu=\frac{w}{L},\end{gathered} \tag{4}$$

where the parameter $\varrho^2$ describes the ring-to-resonator mass ratio, while the parameters $\chi_1^2$ and $\chi_2^2$ account for the rotational-to-translational inertia of the ring and the resonator, respectively. Moreover, the parameters $\eta^2$ and $\mu$ express the material elasticity and (inverse of) slenderness of the flexible ligaments.

Introducing all the nondimensional quantities, the integro-differential equations of motion governing the forced dynamics of the beam lattice metamaterial read

$$\begin{aligned}&\ddot{\tilde{\mathbf{u}}}_{\mathcal{J}}+\int_{-\infty}^{\tilde{t}}\eta^2\kappa_d(\tilde{t}-\tilde{\tau})\tfrac{d}{d\tilde{\tau}}\left(\tilde{\mathbf{u}}_{\mathcal{J}}-\tilde{\mathbf{v}}_{\mathcal{J}}\right)\mathrm{d}\tilde{\tau}+\textstyle\sum_{\mathcal{P}^+_{[\mathrm{j}]}}\tilde{\mathbf{r}}^+_{\mathcal{J}_{[\mathrm{j}]}}+\sum_{\mathcal{P}^-_{[\mathrm{j}]}}\tilde{\mathbf{r}}^-_{\mathcal{J}_{[\mathrm{j}]}}=\tilde{\mathbf{f}}_{\mathcal{J}}, \\ &\chi_1^2\ddot{\phi}_{\mathcal{J}}+\int_{-\infty}^{\tilde{t}}\eta^2\kappa_a(\tilde{t}-\tilde{\tau})\tfrac{d}{d\tilde{\tau}}\left(\phi_{\mathcal{J}}-\theta_{\mathcal{J}}\right)\mathrm{d}\tilde{\tau}+\textstyle\sum_{\mathcal{P}^+_{[\mathrm{j}]}}\tilde{c}^+_{\mathcal{J}_{[\mathrm{j}]}}+\sum_{\mathcal{P}^-_{[\mathrm{j}]}}\tilde{c}^-_{\mathcal{J}_{[\mathrm{j}]}}=\tilde{g}_{\mathcal{J}}, \\ &\varrho^2\ddot{\tilde{\mathbf{v}}}_{\mathcal{J}}+\int_{-\infty}^{\tilde{t}}\eta^2\kappa_d(\tilde{t}-\tilde{\tau})\tfrac{d}{d\tilde{\tau}}\left(\tilde{\mathbf{v}}_{\mathcal{J}}-\tilde{\mathbf{u}}_{\mathcal{J}}\right)\mathrm{d}\tilde{\tau}=\mathbf{0}, \\ &\varrho^2\chi_2^2\ddot{\theta}_{\mathcal{J}}+\int_{-\infty}^{\tilde{t}}\eta^2\kappa_a(\tilde{t}-\tilde{\tau})\tfrac{d}{d\tilde{\tau}}\left(\theta_{\mathcal{J}}-\phi_{\mathcal{J}}\right)\mathrm{d}\tilde{\tau}=0,\end{aligned} \tag{5}$$

where dot here indicates derivative with respect to the nondimensional time $\tilde{t}$. The nondimensional intercellular internal forces exerted on the $\mathcal{J}$-th node are

$$\begin{aligned}\tilde{\mathbf{r}}^+_{\mathcal{J}_{[\mathrm{j}]}}&=\tilde{\mathbf{K}}^+_{[\mathrm{j}]}(\tilde{\mathbf{u}}_{\mathcal{J}_{[\mathrm{j}]}}-\tilde{\mathbf{u}}_{\mathcal{J}^+_{[\mathrm{j}]}})+\tilde{\mathbf{k}}^+_{[\mathrm{j}]}(\phi_{\mathcal{J}_{[\mathrm{j}]}}+\phi_{\mathcal{J}^+_{[\mathrm{j}]}}), \\ \tilde{\mathbf{r}}^-_{\mathcal{J}_{[\mathrm{j}]}}&=\tilde{\mathbf{K}}^-_{[\mathrm{j}]}(\tilde{\mathbf{u}}_{\mathcal{J}_{[\mathrm{j}]}}-\tilde{\mathbf{u}}_{\mathcal{J}^-_{[\mathrm{j}]}})+\tilde{\mathbf{k}}^-_{[\mathrm{j}]}(\phi_{\mathcal{J}_{[\mathrm{j}]}}+\phi_{\mathcal{J}^-_{[\mathrm{j}]}}), \\ \tilde{c}^+_{\mathcal{J}_{[\mathrm{j}]}}&=\tilde{\mathbf{k}}^+_{[\mathrm{j}]}\cdot(\tilde{\mathbf{u}}_{\mathcal{J}_{[\mathrm{j}]}}-\tilde{\mathbf{u}}_{\mathcal{J}^+_{[\mathrm{j}]}})+\tilde{K}_a(\phi_{\mathcal{J}_{[\mathrm{j}]}}+\phi_{\mathcal{J}^+_{[\mathrm{j}]}})+\tilde{K}_\ell(\phi_{\mathcal{J}_{[\mathrm{j}]}}-\phi_{\mathcal{J}^+_{[\mathrm{j}]}}), \\ \tilde{c}^-_{\mathcal{J}_{[\mathrm{j}]}}&=\tilde{\mathbf{k}}^-_{[\mathrm{j}]}\cdot(\tilde{\mathbf{u}}_{\mathcal{J}_{[\mathrm{j}]}}-\tilde{\mathbf{u}}_{\mathcal{J}^-_{[\mathrm{j}]}})+\tilde{K}_a(\phi_{\mathcal{J}_{[\mathrm{j}]}}+\phi_{\mathcal{J}^-_{[\mathrm{j}]}})+\tilde{K}_\ell(\phi_{\mathcal{J}_{[\mathrm{j}]}}-\phi_{\mathcal{J}^-_{[\mathrm{j}]}}),\end{aligned} \tag{6}$$

where the nondimensional stiffness coefficients are

$$\begin{gathered}\tilde{\mathbf{K}}^{\pm}_{[\mathrm{j}]}=\eta^2\delta\mu\left[\left(\mathbf{d}^{\pm}_{[\mathrm{j}]}\otimes\mathbf{d}^{\pm}_{[\mathrm{j}]}\right)+\mu^2\left(\mathbf{t}^{\pm}_{[\mathrm{j}]}\otimes\mathbf{t}^{\pm}_{[\mathrm{j}]}\right)\right], \qquad \tilde{\mathbf{k}}^{\pm}_{[\mathrm{j}]}=\tfrac{1}{2}\alpha\eta^2\delta\mu^3\mathbf{t}^{\pm}_{[\mathrm{j}]}, \\ \tilde{K}_a=\frac{1}{4}\alpha^2\eta^2\delta\mu^3, \qquad \tilde{K}_\ell=\frac{1}{12}(\alpha-2\chi_1)^2\eta^2\delta\mu^3,\end{gathered} \tag{7}$$

where the unit vector $\mathbf{d}^{\pm}_{[\mathrm{j}]}$ indicates the positively or negatively oriented longitudinal local axis of the ligament aligned with the $i_{\mathrm{j}}$ coordination direction, and the unit vector $\mathbf{t}^{\pm}_{[\mathrm{j}]}$ is normal to $\mathbf{d}^{\pm}_{[\mathrm{j}]}$, according to a counter-clockwise axes system (Figure 1c).

The relaxation functions are considered causal and can be formulated by using the Prony series. This formulation corresponds to adopt a Generalized Maxwell constitutive model, which recovers the Standard Linear Solid constitutive model if only one term of the Prony series is considered [45, 58, 59]. Considering only the first term (with infinite relaxation time) and second term (with finite relaxation time $\tilde{t}_r = \eta\omega_r t_r$) of the series, the nondimensional form of the relaxation functions reads

$$\kappa_d(\tilde{t}) = \kappa_{de}\left[1+\beta_d \exp\left(-\frac{\eta\tilde{t}}{\tilde{t}_r}\right)\right], \qquad \kappa_a(\tilde{t}) = \kappa_{ae}\left[1+\beta_a \exp\left(-\frac{\eta\tilde{t}}{\tilde{t}_r}\right)\right]. \tag{8}$$

From the physical viewpoint, the parameters $\kappa_{de}$ and $\kappa_{ae}$ represent the nondimensional stiffnesses at $\tilde{t}\to\infty$ and the *viscosity ratios* $\beta_d$ and $\beta_a$ define the corresponding values $\kappa_{de}(1+\beta_d)$ and $\kappa_{ae}(1+\beta_a)$ for $\tilde{t}=0$. The relaxation functions are featured by higher exponential decay rates for increasing relaxation times.

## 3. In-plane Bloch waves

The propagation of elastic Bloch waves can be studied by recalling first the bilateral Laplace transform $\mathcal{L}[\tilde{q}(\tilde{t})] = \hat{q}(\tilde{s}) = \int_{-\infty}^{\infty}\tilde{q}(\tilde{t})\exp(-\tilde{s}\tilde{t})\,\mathrm{d}\tilde{t}$, where $\tilde{q}(\tilde{t}):\mathbb{R}\to\mathbb{R}$ is a generic time-dependent nondimensional function, $\tilde{s}=s/\omega_r$ is the nondimensional form of the Laplace variable $s\in\mathbb{C}$ and $\hat{q}(\tilde{s}):\mathbb{C}\to\mathbb{C}$ is a complex-valued nondimensional function [60]. Therefore, employing the mathematical properties of the bilateral Laplace transform applied to a convolution product, the equations of motion (5) are transformed as

$$\begin{aligned}
&\tilde{s}^2\hat{\mathbf{u}}_{\mathcal{J}} + \tilde{s}\eta^2\hat{\kappa}_d(\tilde{s})\,(\hat{\mathbf{u}}_{\mathcal{J}}-\hat{\mathbf{v}}_{\mathcal{J}}) + \textstyle\sum_{\mathcal{P}^+_{[\mathrm{j}]}}\hat{\mathbf{r}}^+_{\mathcal{J}_{[\mathrm{j}]}} + \sum_{\mathcal{P}^-_{[\mathrm{j}]}}\hat{\mathbf{r}}^-_{\mathcal{J}_{[\mathrm{j}]}} = \hat{\mathbf{f}}_{\mathcal{J}},\\
&\chi_1^2\tilde{s}^2\hat{\phi}_{\mathcal{J}} + \tilde{s}\eta^2\hat{\kappa}_a(\tilde{s})(\hat{\phi}_{\mathcal{J}}-\hat{\theta}_{\mathcal{J}}) + \textstyle\sum_{\mathcal{P}^+_{[\mathrm{j}]}}\hat{c}^+_{\mathcal{J}_{[\mathrm{j}]}} + \sum_{\mathcal{P}^-_{[\mathrm{j}]}}\hat{c}^-_{\mathcal{J}_{[\mathrm{j}]}} = \hat{g}_{\mathcal{J}},\\
&\varrho^2\tilde{s}^2\hat{\mathbf{v}}_{\mathcal{J}} + \tilde{s}\eta^2\hat{\kappa}_d(\tilde{s})\,(\hat{\mathbf{v}}_{\mathcal{J}}-\hat{\mathbf{u}}_{\mathcal{J}}) = \mathbf{0},\\
&\varrho^2\tilde{s}^2\chi_2^2\hat{\theta}_{\mathcal{J}} + \tilde{s}\eta^2\hat{\kappa}_a(\tilde{s})(\hat{\theta}_{\mathcal{J}}-\hat{\phi}_{\mathcal{J}}) = 0,
\end{aligned} \tag{9}$$

where the bilateral Laplace transforms of the relaxation functions are

$$\hat{\kappa}_d(\tilde{s}) = \kappa_{de}\frac{\eta+\tilde{s}\,(1+\beta_d)\,\tilde{t}_r}{\tilde{s}(\eta+\tilde{s}\,\tilde{t}_r)}, \qquad \hat{\kappa}_a(\tilde{s}) = \kappa_{ae}\frac{\eta+\tilde{s}\,(1+\beta_a)\,\tilde{t}_r}{\tilde{s}(\eta+\tilde{s}\,\tilde{t}_r)} \tag{10}$$

and the bilateral Laplace transforms of inter-cellular internal forces exerted on the $\mathcal{J}$-th node are

$$\begin{aligned}
&\hat{\mathbf{r}}^+_{\mathcal{J}_{[\mathrm{j}]}} = \tilde{\mathbf{K}}^+_{[\mathrm{j}]}(\hat{\mathbf{u}}_{\mathcal{J}_{[\mathrm{j}]}} - \hat{\mathbf{u}}_{\mathcal{J}^+_{[\mathrm{j}]}}) + \tilde{\mathbf{k}}^+_{[\mathrm{j}]}(\hat{\phi}_{\mathcal{J}_{[\mathrm{j}]}} + \hat{\phi}_{\mathcal{J}^+_{[\mathrm{j}]}}),\\
&\hat{\mathbf{r}}^-_{\mathcal{J}_{[\mathrm{j}]}} = \tilde{\mathbf{K}}^-_{[\mathrm{j}]}(\hat{\mathbf{u}}_{\mathcal{J}_{[\mathrm{j}]}} - \hat{\mathbf{u}}_{\mathcal{J}^-_{[\mathrm{j}]}}) + \tilde{\mathbf{k}}^-_{[\mathrm{j}]}(\hat{\phi}_{\mathcal{J}_{[\mathrm{j}]}} + \hat{\phi}_{\mathcal{J}^-_{[\mathrm{j}]}}),\\
&\hat{c}^+_{\mathcal{J}_{[\mathrm{j}]}} = \tilde{\mathbf{k}}^+_{[\mathrm{j}]}\cdot(\hat{\mathbf{u}}_{\mathcal{J}_{[\mathrm{j}]}} - \hat{\mathbf{u}}_{\mathcal{J}^+_{[\mathrm{j}]}}) + \tilde{K}_a(\hat{\phi}_{\mathcal{J}_{[\mathrm{j}]}} + \hat{\phi}_{\mathcal{J}^+_{[\mathrm{j}]}}) + \tilde{K}_\ell(\hat{\phi}_{\mathcal{J}_{[\mathrm{j}]}} - \hat{\phi}_{\mathcal{J}^+_{[\mathrm{j}]}}),\\
&\hat{c}^-_{\mathcal{J}_{[\mathrm{j}]}} = \tilde{\mathbf{k}}^-_{[\mathrm{j}]}\cdot(\hat{\mathbf{u}}_{\mathcal{J}_{[\mathrm{j}]}} - \hat{\mathbf{u}}_{\mathcal{J}^-_{[\mathrm{j}]}}) + \tilde{K}_a(\hat{\phi}_{\mathcal{J}_{[\mathrm{j}]}} + \hat{\phi}_{\mathcal{J}^-_{[\mathrm{j}]}}) + \tilde{K}_\ell(\hat{\phi}_{\mathcal{J}_{[\mathrm{j}]}} - \hat{\phi}_{\mathcal{J}^-_{[\mathrm{j}]}}).
\end{aligned} \tag{11}$$

The transformed algebraic equations (9) govern the forced dynamics of the beam lattice metamaterial in the frequency domain, where $\tilde{s}$ plays the role of complex valued frequency. Then, the spatial periodicity can be treated by introducing the bilateral $\mathcal{Z}$-transform applied to the generic function $q_{\mathcal{J}}:\mathbb{Z}^{n/2}\to\mathbb{C}$

$$\mathcal{Z}[q_{\mathcal{J}}] = \mathcal{Z}[q_{(i_1,\dots,i_{n/2})}] = \sum_{-\infty}^{\infty}\dots\sum_{-\infty}^{\infty} q_{(i_1,\dots,i_{n/2})}z_1^{-i_1}\dots z_{n/2}^{-i_{n/2}} = \breve{q}(z_1\dots z_{n/2}) = \breve{q}(\mathbf{z}), \tag{12}$$

where $\mathbf{z} = (z_1\dots z_{n/2})^{\top}\in\mathbb{C}^{n/2}$ and $\breve{q}(\mathbf{z}):\mathbb{C}^{n/2}\to\mathbb{C}$. Recalling the mathematical property $\mathcal{Z}[q_{(i_1\pm m_1,\dots,i_{n/2}\pm m_{n/2})}] = z_1^{\pm m_1}\dots z_{n/2}^{\pm m_{n/2}}\mathcal{Z}[q_{(i_1,\dots,i_{n/2})}]$ the equations of motion (9) are transformed as

$$\begin{aligned}
&\tilde{s}^2\mathring{\mathbf{u}}(\mathbf{z},\tilde{s}) + \tilde{s}\eta^2\hat{\kappa}_d(\tilde{s})(\mathring{\mathbf{u}}(\mathbf{z},\tilde{s}) - \mathring{\mathbf{v}}(\mathbf{z},\tilde{s})) + \textstyle\sum_{j=1}^{n/2}\mathring{\mathbf{r}}^+_{\mathcal{J}_{[\mathrm{j}]}} + \sum_{j=-n/2}^{-1}\mathring{\mathbf{r}}^-_{\mathcal{J}_{[\mathrm{j}]}} = \mathring{\mathbf{f}}(\mathbf{z},\tilde{s}),\\
&\chi_1^2\tilde{s}^2\mathring{\phi}(\mathbf{z},\tilde{s}) + \tilde{s}\eta^2\hat{\kappa}_a(\tilde{s})(\mathring{\phi}(\mathbf{z},\tilde{s}) - \mathring{\theta}(\mathbf{z},\tilde{s})) + \textstyle\sum_{j=1}^{n/2}\mathring{c}^+_{\mathcal{J}_{[\mathrm{j}]}} + \sum_{j=-n/2}^{-1}\mathring{c}^-_{\mathcal{J}_{[\mathrm{j}]}} = \mathring{g}(\mathbf{z},\tilde{s}),\\
&\varrho^2\tilde{s}^2\mathring{\mathbf{v}}(\mathbf{z},\tilde{s}) + \tilde{s}\eta^2\hat{\kappa}_d(\tilde{s})\,(\mathring{\mathbf{v}}(\mathbf{z},\tilde{s}) - \mathring{\mathbf{u}}(\mathbf{z},\tilde{s})) = \mathbf{0},\\
&\varrho^2\tilde{s}^2\chi_2^2\mathring{\theta}(\mathbf{z},\tilde{s}) + \tilde{s}\eta^2\hat{\kappa}_a(\tilde{s})(\mathring{\theta}(\mathbf{z},\tilde{s}) - \mathring{\phi}(\mathbf{z},\tilde{s})) = 0,
\end{aligned} \tag{13}$$

where $\mathring{q}(\mathbf{z},\tilde{s}) = \mathcal{Z}[\hat{q}_{\mathcal{J}}(\tilde{s})] = \mathcal{Z}[\mathcal{L}[q_{\mathcal{J}}(\tilde{t})]]$ indicates the in-space bilateral $\mathcal{Z}$-transform of the in-time bilateral Laplace transform of the generic function $q_{\mathcal{J}}(\tilde{t})$. The in-space bilateral $\mathcal{Z}$-transform of the inter-cellular internal forces exerted on the $\mathcal{J}$-th node are

$$\begin{aligned}
\mathring{\mathbf{r}}^{+}_{\mathcal{J}_{[\mathrm{j}]}} &= (1-z_j)\tilde{\mathbf{K}}^{+}_{[\mathrm{j}]}\mathring{\mathbf{u}}(\mathbf{z},\tilde{s}) + (1+z_j)\tilde{\mathbf{k}}^{+}_{[\mathrm{j}]}\mathring{\phi}(\mathbf{z},\tilde{s}),\\
\mathring{\mathbf{r}}^{-}_{\mathcal{J}_{[\mathrm{j}]}} &= (1-z_j^{-1})\tilde{\mathbf{K}}^{-}_{[\mathrm{j}]}\mathring{\mathbf{u}}(\mathbf{z},\tilde{s}) + (1+z_j^{-1})\tilde{\mathbf{k}}^{-}_{[\mathrm{j}]}\mathring{\phi}(\mathbf{z},\tilde{s}),\\
\mathring{c}^{+}_{\mathcal{J}_{[\mathrm{j}]}} &= (1-z_j)\tilde{\mathbf{k}}^{+}_{[\mathrm{j}]}\cdot\mathring{\mathbf{u}}(\mathbf{z},\tilde{s}) + (1-z_j)\tilde{K}_a\mathring{\phi}(\mathbf{z},\tilde{s}) + (1-z_j)\tilde{K}_\ell\mathring{\phi}(\mathbf{z},\tilde{s}),\\
\mathring{c}^{-}_{\mathcal{J}_{[\mathrm{j}]}} &= (1-z_j^{-1})\tilde{\mathbf{k}}^{-}_{[\mathrm{j}]}\cdot\mathring{\mathbf{u}}(\mathbf{z},\tilde{s}) + (1-z_j^{-1})\tilde{K}_a\mathring{\phi}(\mathbf{z},\tilde{s}) + (1-z_j^{-1})\tilde{K}_\ell\mathring{\phi}(\mathbf{z},\tilde{s}).
\end{aligned} \tag{14}$$

Collecting the doubly-transformed displacements in the six-by-one vector $\mathring{\mathbf{U}}(\mathbf{z},\tilde{s}) = (\mathring{\mathbf{u}}(\mathbf{z},\tilde{s})\ \mathring{\phi}(\mathbf{z},\tilde{s})\ \mathring{\mathbf{v}}(\mathbf{z},\tilde{s})\ \mathring{\theta}(\mathbf{z},\tilde{s}))^{\top}$ and the doubly-transformed forces in the six-by-one vector $\mathring{\mathbf{F}}(\mathbf{z},\tilde{s}) = (\mathring{\mathbf{f}}(\mathbf{z},\tilde{s})\ \mathring{g}(\mathbf{z},\tilde{s})\ \mathbf{0}\ 0)^{\top}$, the linear algebraic equations (13) can conveniently be expressed in the matrix form

$$\mathbf{C}(\mathbf{z},\tilde{s})\mathring{\mathbf{U}}(\mathbf{z},\tilde{s}) = \mathring{\mathbf{F}}(\mathbf{z},\tilde{s}), \tag{15}$$

where the six-by-six matrix $\mathbf{C}(\mathbf{z},\tilde{s})$ is the dynamic stiffness matrix and can be expressed in the form

$$\mathbf{C}(\mathbf{z},\tilde{s}) = \begin{bmatrix}
\mathbf{A}(\mathbf{z},\tilde{s}) + \tilde{s}^2\mathbf{I} & \mathbf{a}^{-}(\mathbf{z}) & -\tilde{s}\eta^2\hat{\kappa}_d(\tilde{s})\mathbf{I} & \mathbf{0}\\
\mathbf{a}^{+}(\mathbf{z}) & B(\mathbf{z},\tilde{s}) + \tilde{s}^2\chi_1^2 & \mathbf{0} & -\tilde{s}\eta^2\hat{\kappa}_a(\tilde{s})\\
-\tilde{s}\eta^2\hat{\kappa}_d(\tilde{s})\mathbf{I} & \mathbf{0} & \tilde{s}\eta^2\hat{\kappa}_d(\tilde{s})\mathbf{I} + \tilde{s}^2\varrho^2\mathbf{I} & \mathbf{0}\\
\mathbf{0} & -\tilde{s}\eta^2\hat{\kappa}_a(\tilde{s}) & \mathbf{0} & \tilde{s}\eta^2\hat{\kappa}_a(\tilde{s}) + \tilde{s}^2\varrho^2\chi_2^2
\end{bmatrix}, \tag{16}$$

with the auxiliary quantities

$$\begin{aligned}
\mathbf{A}(\mathbf{z},\tilde{s}) &= \tilde{s}\eta^2\hat{\kappa}_d(\tilde{s})\mathbf{I} + \textstyle\sum_{j=1}^{n/2}\left[(1-z_j)\tilde{\mathbf{K}}^{+}_{[\mathrm{j}]}\right] + \sum_{j=-n/2}^{-1}\left[(1-z_j^{-1})\tilde{\mathbf{K}}^{-}_{[\mathrm{j}]}\right],\\
\mathbf{a}^{-}(\mathbf{z}) &= \textstyle\sum_{j=1}^{n/2}\left[(1+z_j)\tilde{\mathbf{k}}^{+}_{[\mathrm{j}]}\right] + \sum_{j=-n/2}^{-1}\left[(1+z_j^{-1})\tilde{\mathbf{k}}^{-}_{[\mathrm{j}]}\right],\\
\mathbf{a}^{+}(\mathbf{z}) &= \textstyle\sum_{j=1}^{n/2}\left[(1-z_j)\tilde{\mathbf{k}}^{+}_{[\mathrm{j}]}\right] + \sum_{j=-n/2}^{-1}\left[(1-z_j^{-1})\tilde{\mathbf{k}}^{-}_{[\mathrm{j}]}\right],\\
B(\mathbf{z},\tilde{s}) &= \tilde{s}\eta^2\hat{\kappa}_a(\tilde{s}) + \textstyle\sum_{j=1}^{n/2}\left[(1+z_j)\tilde{K}_a + (1-z_j)\tilde{K}_\ell\right] + \sum_{j=-n/2}^{-1}\left[(1+z_j^{-1})\tilde{K}_a + (1-z_j^{-1})\tilde{K}_\ell\right]
\end{aligned} \tag{17}$$

and $\mathbf{I}$ indicating identity matrices. Therefore, mapping the complex variables $z_j$ (for $j = 1, ..., n/2$) in the unitary circle as $z_j = \exp[\imath(\mathbf{n}_{[\mathrm{j}]}\cdot\mathbf{b})]$, the equation (15) can be expressed in the form

$$\mathbf{C}(\mathbf{b},\tilde{s})\mathring{\mathbf{U}}(\mathbf{b},\tilde{s}) = \mathring{\mathbf{F}}(\mathbf{b},\tilde{s}), \tag{18}$$

where $\mathbf{n}_{[\mathrm{j}]}$ indicates the unit vector along the $j$-th coordination direction, while $\mathbf{b} = (\beta_1\ \beta_2)^{\top}$ plays the role of nondimensional real-valued wavevector.

## 4. Free wave propagation

For the free wave propagation, the complex-valued dispersion relations $\tilde{s}(\mathbf{b})$ can be determined by stating the rational eigenvalue problem associated to the homogeneous equation of motion

$$\mathbf{C}(\mathbf{b},\tilde{s})\mathring{\mathbf{U}}(\mathbf{b},\tilde{s}) = \mathbf{0}, \tag{19}$$

obtained by zeroing the generalized external forces $\mathring{\mathbf{F}}(\mathbf{b},\tilde{s})$. The eigenvalue problem consists in searching for non-trivial $\mathring{\mathbf{U}}$-solutions by requiring that the $\mathbf{C}(\mathbf{b},\tilde{s})$-matrix is singular for certain values (eigenvalues) of the $\tilde{s}$-unknown. As preliminary remark, it must be highlighted that the characteristic function $F(\mathbf{b},\tilde{s}) = \det\mathbf{C}(\mathbf{b},\tilde{s})$ is a rational function of the unknown $\tilde{s}$. Therefore, the singularity conditions $F(\mathbf{b},\tilde{s}) = 0$ may return a number of eigenvalues $\tilde{s}(\mathbf{b})$ higher than the model dimension.

Two strategies can be explored to attack the rational eigenvalue problem. The first is to seek for the exact solutions $\tilde{s}(\mathbf{b})$ by algebraic manipulations of the homogeneous equation (19), according to a sort of *de-rationalization* procedure [61]. The second is to seek for the solutions $\tilde{s}(\mathbf{b})$ of the approximate eigenvalue problem obtained by expanding the rational relaxation functions $\hat{\kappa}_d(\tilde{s})$ and $\hat{\kappa}_a(\tilde{s})$ in Laurent series of the $\tilde{s}$-variable and truncating the series at a suited order. Due to the approximation inherent to the series truncation, the second strategy requires a complementary discussion about the solution convergence. Specifically, the number of eigenvalues depends on the order of the series expansion, but the boundary of the convergence region can be employed to exclude outlier eigenvalues. Independently of the solving strategy, the solutions of the *derationalized eigenvalue problem* (Subsection 4.1) or the *approximate eigenvalue problem* (Subsection 4.2) return the complex-valued dispersion spectrum in the nondimensional first Brillouin zone $\mathcal{B}$, spanned by the wavevector $\mathbf{b}$.

### *4.1. De-rationalized eigenvalue problem*

According to the first strategy, the rational eigenvalue problem can be attacked by conveniently re-formulating the equation (19) in the simpler form

$$\left(\tilde{s}^2\mathbf{M}+\frac{\eta^2\tilde{t}_r}{\eta+\tilde{s}\tilde{t}_r}\left(\tilde{s}\mathbf{G}_1+\mathbf{G}_0\right)+\mathbf{H}(\mathbf{b})\right)\mathring{\mathbf{U}}(\mathbf{b},\tilde{s})=\mathbf{0}, \tag{20}$$

where the matrices are

$$\mathbf{M}=\begin{bmatrix}\mathbf{I} & \mathbf{0} & \mathbf{0} & \mathbf{0}\\ \mathbf{0} & \chi_1^2 & \mathbf{0} & 0\\ \mathbf{0} & \mathbf{0} & \varrho^2\mathbf{I} & \mathbf{0}\\ \mathbf{0} & 0 & \mathbf{0} & \varrho^2\chi_2^2\end{bmatrix},\qquad \mathbf{G}_1=\begin{bmatrix}\kappa_{de}(1+\beta_d)\mathbf{I} & \mathbf{0} & -\kappa_{de}(1+\beta_d)\mathbf{I} & \mathbf{0}\\ \mathbf{0} & \kappa_{ae}(1+\beta_a) & \mathbf{0} & -\kappa_{ae}(1+\beta_a)\\ -\kappa_{de}(1+\beta_d)\mathbf{I} & \mathbf{0} & \kappa_{de}(1+\beta_d)\mathbf{I} & \mathbf{0}\\ \mathbf{0} & -\kappa_{ae}(1+\beta_a) & \mathbf{0} & \kappa_{ae}(1+\beta_a)\end{bmatrix}, \tag{21}$$

$$\mathbf{G}_0=\frac{\eta}{\tilde{t}_r}\begin{bmatrix}\kappa_{de}\mathbf{I} & \mathbf{0} & -\kappa_{de}\mathbf{I} & \mathbf{0}\\ \mathbf{0} & \kappa_{ae} & \mathbf{0} & -\kappa_{ae}\\ -\kappa_{de}\mathbf{I} & \mathbf{0} & \kappa_{de}\mathbf{I} & \mathbf{0}\\ \mathbf{0} & -\kappa_{ae} & \mathbf{0} & \kappa_{ae}\end{bmatrix},\qquad \mathbf{H}(\mathbf{b})=\begin{bmatrix}\mathbf{A}_0(\mathbf{b}) & \mathbf{a}^-(\mathbf{b}) & \mathbf{0} & \mathbf{0}\\ \mathbf{a}^+(\mathbf{b}) & B_0(\mathbf{b}) & \mathbf{0} & 0\\ \mathbf{0} & \mathbf{0} & \mathbf{0} & \mathbf{0}\\ \mathbf{0} & 0 & \mathbf{0} & 0\end{bmatrix},$$

and the auxiliary terms are

$$\begin{aligned}\mathbf{A}_0(\mathbf{b})&=\textstyle\sum_{j=1}^{n/2}\left[E^{\mp}_{[\mathrm{j}]}(\mathbf{b})\tilde{\mathbf{K}}^{+}_{[\mathrm{j}]}\right]+\sum_{j=-n/2}^{-1}\left[E^{=}_{[\mathrm{j}]}(\mathbf{b})\tilde{\mathbf{K}}^{-}_{[\mathrm{j}]}\right],\\ B_0(\mathbf{b})&=\textstyle\sum_{j=1}^{n/2}\left[E^{\#}_{[\mathrm{j}]}(\mathbf{b})\tilde{K}_a+E^{\mp}_{[\mathrm{j}]}(\mathbf{b})\tilde{K}_\ell\right]+\sum_{j=-n/2}^{-1}\left[E^{\pm}_{[\mathrm{j}]}(\mathbf{b})\tilde{K}_a+E^{=}_{[\mathrm{j}]}(\mathbf{b})\tilde{K}_\ell\right],\end{aligned} \tag{22}$$

where the auxiliary parameters $E^{\#}_{[\mathrm{j}]}(\mathbf{b})=1+\exp[\imath(\mathbf{n}_{[\mathrm{j}]}\cdot\mathbf{b})]$, $E^{\pm}_{[\mathrm{j}]}(\mathbf{b})=1+\exp[-\imath(\mathbf{n}_{[\mathrm{j}]}\cdot\mathbf{b})]$, $E^{\mp}_{[\mathrm{j}]}(\mathbf{b})=1-\exp[\imath(\mathbf{n}_{[\mathrm{j}]}\cdot\mathbf{b})]$, $E^{=}_{[\mathrm{j}]}(\mathbf{b})=1-\exp[-\imath(\mathbf{n}_{[\mathrm{j}]}\cdot\mathbf{b})]$ and the solving procedure is reported in AppendixA. It is worth remarking that the number of complex-valued eigenvalues is $n_e=15$ (after exclusion of the non-admissible multiple solution $\tilde{s}=-\eta/\tilde{t}_r$), that is, larger than the number of degrees-of-freedom of the periodic cell.

### *4.2. Approximate eigenvalue problem*

According to the second strategy, the rational eigenvalue problem can be attacked by approximating the Laplace transforms of the relaxation functions $\hat{\kappa}_d(\tilde{s})$ and $\hat{\kappa}_a(\tilde{s})$ with their respective Laurent series around the polar singularity in $\tilde{s}=0$ and truncating at the $h$-th order

$$\hat{\kappa}_d(\tilde{s})\simeq\frac{\kappa_{de}}{\tilde{s}}\left[1-\textstyle\sum_{j=1}^{h}(-1)^j\beta_d\left(\frac{\tilde{s}\tilde{t}_r}{\eta}\right)^j\right],\qquad \hat{\kappa}_a(\tilde{s})\simeq\frac{\kappa_{ae}}{\tilde{s}}\left[1-\textstyle\sum_{j=1}^{h}(-1)^j\beta_a\left(\frac{\tilde{s}\tilde{t}_r}{\eta}\right)^j\right], \tag{23}$$

whose radius of convergence is inversely proportional to the relaxation time according to the ratio $\eta/\tilde{t}_r$ (see for instance [60]). From the physical viewpoint, it is worth noting that the simple case of purely elastic ring-resonator coupling can be recovered (with stiffnesses $\kappa_{de}$, $\kappa_{ae}$) if the sum is neglected, while the

particular case of Kelvin-Voigt visco-elastic coupling can be recovered (with viscosity coefficients $\eta\kappa_{de}\beta_d\tilde{t}_r$, $\eta\kappa_{ae}\beta_d\tilde{t}_r$) by truncating at the lowest order of the series ($h=1$). For higher orders of the series ($h>1$), the eigenproblem can be solved by conveniently re-formulating the equation (19) in the simpler form

$$\left(\sum_{j=0}^{h}\mathbf{C}_j(\mathbf{b})\tilde{s}^j\right)\mathring{\mathbf{U}}(\mathbf{b},\tilde{s})=\left(\tilde{s}^2\mathbf{M}+\sum_{j=0}^{h}\mathbf{N}_j\left(\tilde{s}\mathbf{G}_1+\mathbf{G}_0\right)\tilde{s}^j+\mathbf{H}(\mathbf{b})\right)\mathring{\mathbf{U}}(\mathbf{b},\tilde{s})=\mathbf{0}, \tag{24}$$

with the matrix coefficient in the sum

$$\mathbf{N}_j=(-1)^j\frac{\tilde{t}_r^{j+1}}{\eta^{j-1}}\mathbf{I}, \tag{25}$$

whose solving procedure is reported in AppendixB. It can be worth remarking that the number of complex-valued eigenvalues (before discriminating about the their mathematical admissibility) can be verified to be $n_e=6\times2+3(h-1)$, that is, possibly larger than the number of degrees-of-freedom of the periodic cell.

### *4.3. Quadrilateral beam lattice*

In order to specify the formulation for a particular microstructural topology of interest, the mechanical metamaterial based on the quadrilateral beam lattice is considered. To this purpose, it is sufficient to particularize the matrix $\mathbf{H}(\mathbf{b})$ by defining the submatrices

$$\begin{aligned}
\mathbf{A}_0(\mathbf{b})&=\begin{bmatrix}2\delta\mu\eta^2\left(1+\mu^2-C_1(\mathbf{b})\right) & 0\\ 0 & 2\delta\mu\eta^2\left(1+\mu^2-C_2(\mathbf{b})\right)\end{bmatrix},\\
\mathbf{a}^-(\mathbf{b})&=\begin{bmatrix}-\imath\delta\alpha\eta^2\mu^3\sin\beta_2 & \imath\delta\alpha\eta^2\mu^3\sin\beta_1\end{bmatrix}^\top,\\
\mathbf{a}^+(\mathbf{b})&=\begin{bmatrix}\imath\delta\alpha\eta^2\mu^3\sin\beta_2 & -\imath\delta\alpha\eta^2\mu^3\sin\beta_1\end{bmatrix},\\
B_0(\mathbf{b})&=\tfrac{1}{3}\delta\eta^2\mu^3\left(4(\alpha^2-\alpha\chi_1+\chi_1^2)+(\alpha^2+2\chi_1\alpha-2\chi_1^2)C_3(\mathbf{b})\right),
\end{aligned} \tag{26}$$

where the auxiliary parameters are $C_1(\mathbf{b})=\cos\beta_1+\mu^2\cos\beta_2$, $C_2(\mathbf{b})=\cos\beta_2+\mu^2\cos\beta_1$, $C_3(\mathbf{b})=\cos\beta_1+\cos\beta_2$, where the wavevector $\mathbf{b}$ spans the first Brillouin zone $\mathcal{B}=[-\pi,\pi]\times[-\pi,\pi]$.

The complex-valued spectra defined by the dispersion functions $\tilde{s}_n(\xi)$ are considered, where the normalized complex frequency $\tilde{s}_n=\tilde{s}/\eta$ is introduced and the curvilinear abscissa $\xi\in[0,\pi(2+\sqrt{2})]$ is employed to span the closed boundary $\partial\mathcal{B}$ of the triangular subdomain $\mathcal{B}_1\subset\mathcal{B}$, limited by the vertices $\Xi_1,\Xi_2,\Xi_3$ (pointed by the nondimensional wavevectors $\mathbf{b}_1=(0\ 0)^\top$, $\mathbf{b}_1=(0\ \pi)^\top$, $\mathbf{b}_3=(\pi\ \pi)^\top$ respectively). The real and imaginary parts of the complex frequency $\tilde{s}_n(\xi)$, which can be referred to as wave *damping* and wave *frequency* in the following, are related to the propagation in space and the attenuation in time of the mono-harmonic wave traveling through the metamaterial. Negative real parts of the complex frequency correspond to in-time exponentially decaying amplitudes of the propagating wave.

A prototypical metamaterial characterized by technically feasible values of the mechanical parameters $\varrho^2=25/6$, $\chi_1^2=1/25$, $\chi_2^2=1/200$, $\alpha=1$, $\delta=1$, $\mu=1/10$ is considered as reference case. The limit condition of undamped resonators (metamaterial $\mathcal{M}_e$) and the reference condition of damped resonators with nominal visco-elastic parameters $\tilde{t}_r=1/5$, $\kappa_{de}=7/20$, $\kappa_{ae}=4/625$ and $\beta_d=\beta_a=10$ (metamaterial $\mathcal{M}_d$) are analyzed. The spectra related to the metamaterials $\mathcal{M}_e$ and $\mathcal{M}_d$ are reported in Figure 2. Specifically, the spectrum of the damped metamaterial is obtained through the de-rationalization procedure presented in Subsection 4.1. The eigenvalue problem of the undamped metamaterial $\mathcal{M}_e$ presents six pairs of conjugate purely imaginary solutions. The corresponding spectrum is composed by six dispersion curves, or branches, in the *imaginary plane* (orange dots in Figure 2a), one for each dispersion function $\tilde{s}_n(\xi)$ with positive imaginary part. The spectral branches with null imaginary part at the limit of long wavelengths ($\xi=0$) are referred to as *acoustic branches*, the others as *optical branches*. From the physical viewpoint, these spectral branches correspond to waves propagating without attenuation. A full large-amplitude stop band (or band gap) separates the three low-frequency (two acoustic and one optical) dispersion curves from the three high-frequency (optical) dispersion curves (Figure 2b). It can be verified that the low-frequency curves are

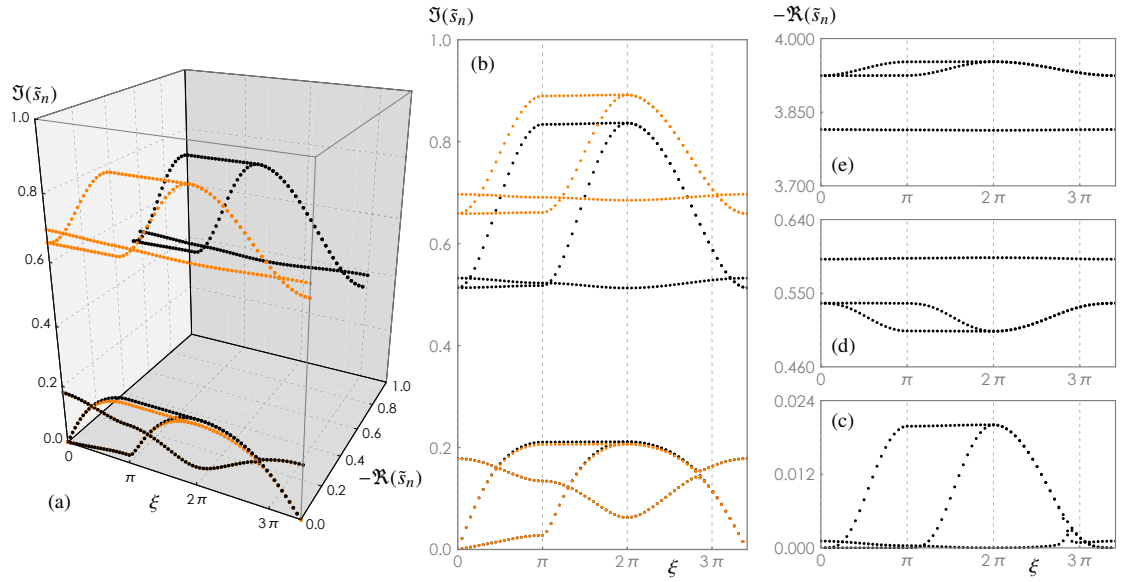


Figure 2: Comparison between the dispersion spectra of the undamped metamaterial $\mathcal{M}_e$ (orange dots) and the damped metamaterial $\mathcal{M}_d$ (black dots): (a) complex-valued spectra: (b) imaginary parts of the spectra, (c),(d),(e) real parts of the spectra.

associated to waveforms systematically localized in the ring displacements (*ring polarization*), with quasi-static contribution of the generalized resonator displacements. Differently, the high-frequency curves are associated to waveforms mainly localized in the resonator displacements (*resonator polarization*).

The eigenvalue problem of the damped metamaterial $\mathcal{M}_d$ presents six pairs of complex conjugate solutions plus three purely real and negative solutions. Therefore, the spectrum has both a real and an imaginary part (black dots in Figure 2a). Focusing first on the complex conjugate solutions with positive imaginary parts, the three curves in the low frequency range can be conventionally referred to as spectral branches of *weak-attenuation*, since they are dominated by the imaginary part of the complex frequency, with minimal participation of its real part (low real values in Figure 2c). It can be verified that the slight dynamic interaction between the ring and the resonator, caused by the ring polarization, reduces the attenuation offered by the viscoelastic coupling. Consequently, no appreciable differences can be recognized in the low-frequency spectra of the damped and undamped metamaterials. The remaining three curves in the high frequency range can be conventionally referred to as spectral branches of *strong-attenuation*, since they are significantly contributed by the real part of the complex frequency (non-negligible real values in Figure 2d). It can be verified that the strong ring-resonator interaction caused by the resonator polarization increases the attenuation offered by the viscoelastic coupling. As important remark, the strong frequency reduction caused by the viscoelastic coupling in the damped metamaterial causes a marked decrement in the stop bandwidth, intended as the gap between the imaginary parts of the low-frequency and the high-frequency dispersion curves (Figure 2b). Focusing on the three real negative solutions, the corresponding curves lie in the high-damping range of the *real plane* (high real values in Figure 2e) and can be conventionally referred to as spectral branches of *pure-attenuation* or *pure damping*. As minor remarks, some branches associated to multiple real-valued eigenvalues must be discarded, because they violate the conditions of non singularity (see AppendixB). From the physical viewpoint, pure-attenuation branches correspond to waves non-propagating in space but highly damped in time. As complementary remarks, synthesized from a wide parametric analysis (here not reported for the sake of synthesis), slight changes in the mechanical properties of the viscoelastic coupling do not modify the spectral characteristics of the damped metamaterial $\mathcal{M}_d$ from the qualitative viewpoint, if the condition of undercritical damping remains satisfied. From the quantitative viewpoint, increments in the relaxation time $\tilde{t}_r$ systematically tends to increase the wave damping of both the weak-attenuation and the strong-attenuation branches of the spectrum. Nonetheless, increasing relaxation times causes also the frequencies of strong-attenuation branches to reduce faster than those of the weak attenuation branches, possibly leading – for sufficiently high relaxation times – to the

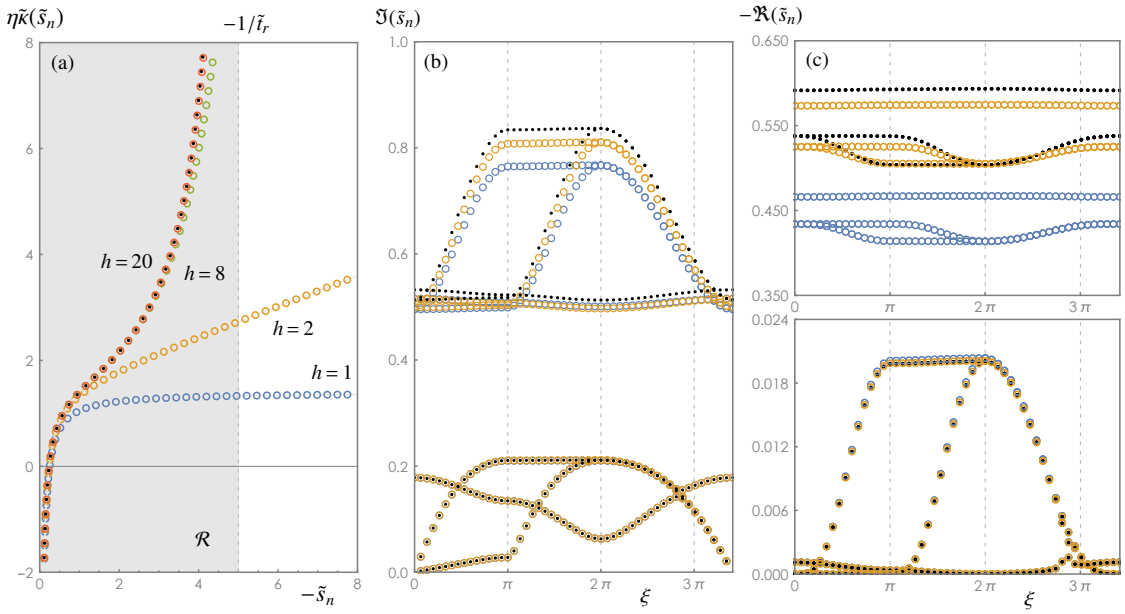


Figure 3: Dispersion spectrum of the damped metamaterial $\mathcal{M}_d$ (black dots) compared with its $h$-order approximations (circles): (a) relaxation functions, (b) imaginary parts of the spectrum, (c) real parts of the spectrum.

so-called *branch overtaking* phenomenon [48]. Similar spectral effects can be observed under reduction of the viscosity ratios $\beta_d$ and $\beta_a$. As final remark, the pure-attenuation branches turn out to be highly sensitive to the mechanical properties of the viscoelastic coupling, with significantly higher damping associated to decrements in the relaxation time.

The complex-valued spectrum obtained through the de-rationalization procedure can also be compared with the complex-valued spectrum obtainable with the approximation procedure presented in Subsection 4.2. Specifically, the comparison can be performed with the complex-valued spectra associated to increasing maximum $h$-orders of the truncated Laurent series (23) approximating the relaxation functions $\hat{\kappa}_d(\tilde{s}_n)$ and $\hat{\kappa}_a(\tilde{s}_n)$. First, the accuracy achievable in the approximation of the real part of the function $\hat{\kappa}_d(\tilde{s}_n)$ versus the real part of the variable $\tilde{s}_n$ is illustrated in Figure 3a. In particular, the comparison with the exact function allows to appreciate the convergence of the series within the limits of its region of convergence $\mathcal{R}$ (gray region), centered at the polar singularity $\tilde{s}_n = 0$ and bounded by the radius $1/\tilde{t}_r$. Low-order approximations ($h = 1, 2$) can be recognized to provide a good accuracy only in the closeness of the singularity (*short-range* accuracy). High-order approximations ($h = 8, 20$) are necessary to ensure a good accuracy also in the closeness of the $\mathcal{R}$-boundary (*long-range* accuracy). Second, the real and imaginary parts of the complex-valued spectra associated to increasing orders of approximations are directly compared (Figures 3b,c). It is worth recalling that the number of eigenvalues $n_e$ depends on the approximation order and can be lower ($h = 1$), equal ($h = 2$) or higher ($h > 2$) than the actual number of eigenvalues. Focusing first on the complex conjugate solutions, it can be immediately recognized that the real and imaginary parts of the weak-attenuation branches of the damped metamaterial spectrum are accurately described by low-order approximations ($h = 1, 2$). This result is fully consistent with the short-range accuracy of the low-order approximations in the convergence analysis concerning the relaxation functions. Lower accuracy can be noted in the approximation of the strong-attenuation branches, although a rapid monotonic convergence can be appreciated. As important remark, low order approximations determine a certain underestimation of the stop bandwidth (Figures 3b). The pure-attenuation branches are absent in the lowest order approximation ($h = 1$) and systematically overestimated by other low-order approximations ($h = 2, 3, ...$). Indeed, the pure-attenuation branches lie in the external part of the convergence region $\mathcal{R}$, so that high orders of approximations are required to achieve a sufficient accuracy in their approximation, consistently with the long-range accuracy (Figure 3a). Specifically, high order of approximations ($h = 8, 20$) return a large num-

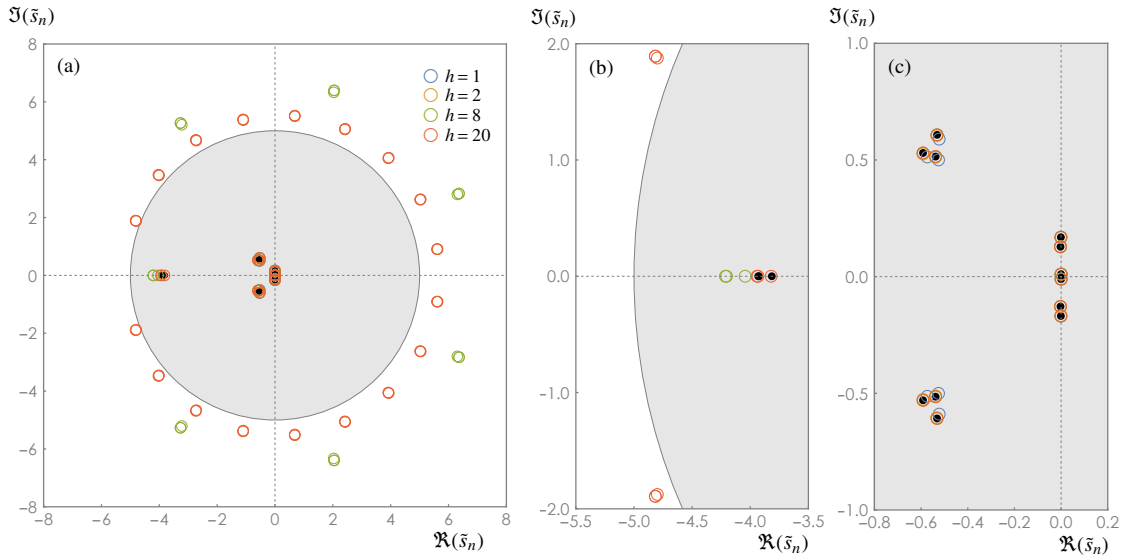


Figure 4: Dispersion spectrum of the damped metamaterial $\mathcal{M}_d$ (black dots) compared with its $h$-order approximations (circles): (a) complex frequencies at the limit of long wavelengths, (b) window on the complex frequencies of the pure-attenuation branches, (c) window on the complex frequencies of the weak-attenuation and strong-attenuation branches.

ber of eigenvalues ($n_e > 15$), many of which must be discarded because they either have a real positive part or anyway lie outside the convergence region. To exemplify, all the discardable eigenvalues lie outside the circular $\mathcal{R}$-region in Figure 4a, illustrating a section of the metamaterial spectrum at the limit of long wavelengths ($\xi = 0$). The other eigenvalues either almost perfectly sit on the weak and strong-attenuation branches (Figure 4b), or converge to the pure attenuation branches (Figure 4c).

## 5. Forced wave propagation

Considering generic external forces $\mathring{\mathbf{F}}(\mathbf{z}, \tilde{s})$ acting on the mechanical metamaterial, the forced response $\mathring{\mathbf{U}}(\mathbf{z}, \tilde{s})$ can be obtained from equation (15) by inverting the dynamic stiffness matrix

$$\mathring{\mathbf{U}}(\mathbf{z}, \tilde{s}) = \mathbf{C}^{-1}(\mathbf{z}, \tilde{s})\mathring{\mathbf{F}}(\mathbf{z}, \tilde{s}) = \mathbf{D}(\mathbf{z}, \tilde{s})\mathring{\mathbf{F}}(\mathbf{z}, \tilde{s}), \tag{27}$$

where the six-by-six matrix $\mathbf{D}(\mathbf{z}, \tilde{s})$ is the dynamic compliance (or flexibility) matrix. Therefore, mapping the complex components $z_j$ (for $j = 1, ..., n/2$) of the vector $\mathbf{z}$ in the unitary circle as $z_j = \exp[\imath(\mathbf{n}_{[j]} \cdot \mathbf{b})]$, the equation (27) can also be expressed in the form

$$\mathring{\mathbf{U}}(\mathbf{b}, \tilde{s}) = \mathbf{C}^{-1}(\mathbf{b}, \tilde{s})\mathring{\mathbf{F}}(\mathbf{b}, \tilde{s}) = \mathbf{D}(\mathbf{b}, \tilde{s})\mathring{\mathbf{F}}(\mathbf{b}, \tilde{s}), \tag{28}$$

which can alternately obtained by directly inverting equation (18). Then, the forced response at the $\mathcal{J}$-th lattice node can be obtained by applying the inverse bilateral $\mathcal{Z}$-transform to equation (27), yielding

$$\mathcal{Z}^{-1}[\mathring{\mathbf{U}}(\mathbf{z}, \tilde{s})] = \frac{1}{(2\pi\imath)^{n/2}} \oint_{\Gamma_{n/2}} ... \oint_{\Gamma_1} \mathring{\mathbf{U}}(z_1, ..., z_{n/2}, \tilde{s})\, z_1^{(i_1-1)} ... z_{n/2}^{(i_{n/2}-1)} \mathrm{d}z_1 ... \mathrm{d}z_{n/2} = \hat{\mathbf{U}}_{(i_1,...,i_{n/2})}(\tilde{s}) = \hat{\mathbf{U}}_{\mathcal{J}}(\tilde{s}), \tag{29}$$

where $\Gamma_1, ..., \Gamma_{n/2}$ are closed paths in the region of convergence of $\mathring{\mathbf{U}}(\mathbf{z}, \tilde{s})$. Specifically, $\Gamma_j$ is a counter-clockwise closed path encircling the origin of the complex plane $z_j$ with fixed $z_\ell$ (for $\ell \neq j$). The same result could be achieved by applying the inverse discrete Fourier transform to equation (28), yielding

$$\mathcal{F}_d^{-1}[\mathring{\mathbf{U}}(\mathbf{b}, \tilde{s})] = \frac{1}{(2\pi)^{n/2}} \int_{\mathcal{B}} \mathring{\mathbf{U}}(\mathbf{b}, \tilde{s})\, \mathrm{e}^{\imath(i_1-1)(\mathbf{n}_{[1]}\cdot\mathbf{b})} ... \mathrm{e}^{\imath(i_1-1)(\mathbf{n}_{[n/2]}\cdot\mathbf{b})} \mathrm{d}\mathbf{b} = \hat{\mathbf{U}}_{(i_1,...,i_{n/2})}(\tilde{s}) = \hat{\mathbf{U}}_{\mathcal{J}}(\tilde{s}), \tag{30}$$

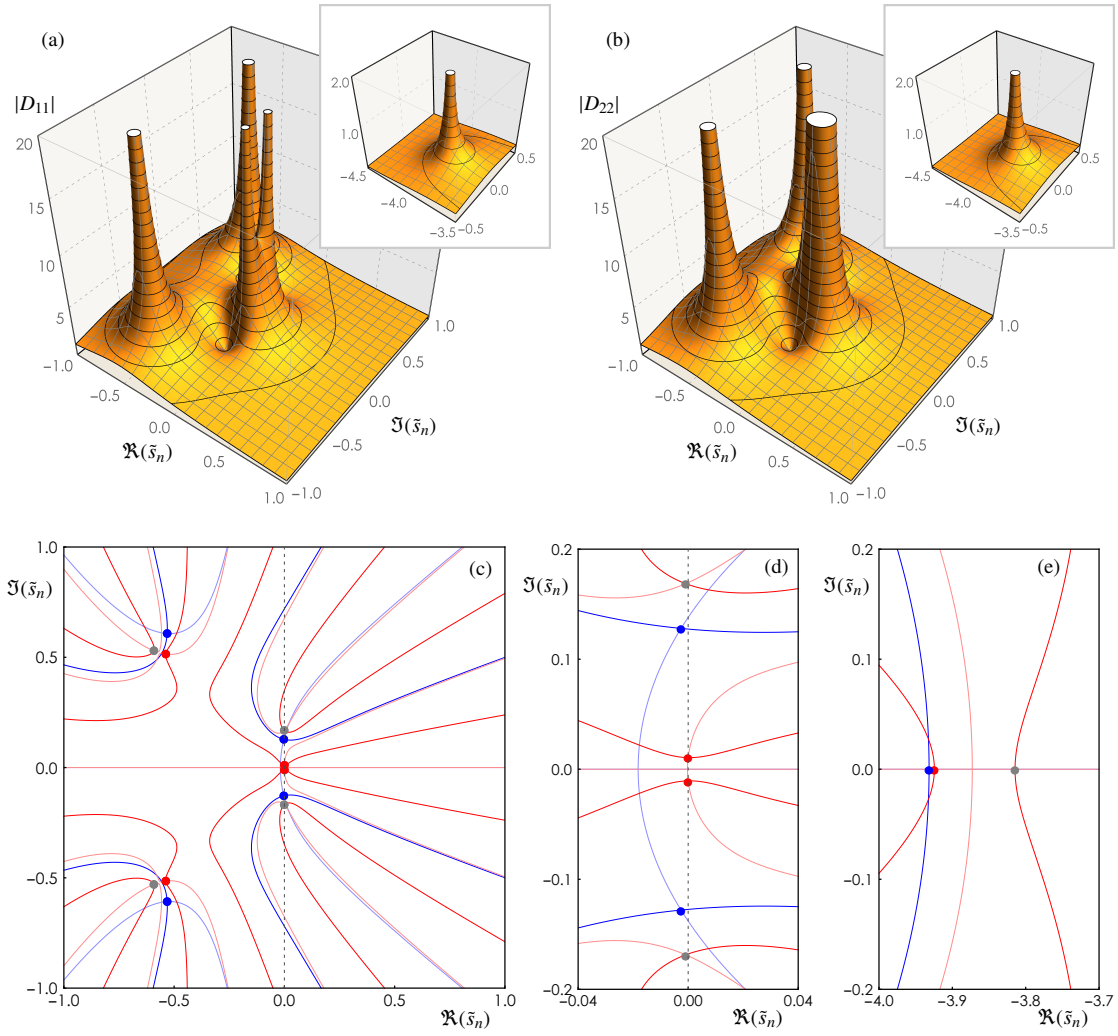


Figure 5: Compliance matrix of the damped metamaterial $\mathcal{M}_d$ for fixed wavevector $\mathbf{b}_*$: (a) magnitude of the coefficients $D_{11}$ in the space of complex frequencies,(b) magnitude of the coefficients $D_{22}$ in the space of complex frequencies, (b),(c),(d) singularity points of the coefficient $D_{11}$ (blue dots) and $D_{22}$ (red dots) in the space of complex frequencies.

which entails integrating over the first Brillouin zone $\mathcal{B}$. Finally, in order to come back in the time domain, the application of the inverse bilateral Laplace transform allows to obtain

$$\mathcal{L}^{-1}[\hat{\mathbf{U}}_{\mathcal{J}}(\tilde{s})] = \frac{1}{(2\pi\imath)^{n/2}} \int_{r-\imath\,\infty}^{r+\imath\,\infty} \hat{\mathbf{U}}_{\mathcal{J}}(\tilde{s})\, \mathrm{e}^{\tilde{s}\tilde{t}} \mathrm{d}\tilde{s} = \tilde{\mathbf{U}}_{\mathcal{J}}(\tilde{t})\,, \qquad r \in \mathbb{R}, \tag{31}$$

where $\tilde{\mathbf{U}}_{\mathcal{J}}(\tilde{t})$ collects the nondimensional time-dependent displacements. The integral in equation (31) can be evaluated as $\tilde{\mathbf{U}}_{\mathcal{J}}(\tilde{t}) = \sum \mathrm{Res}[\tilde{\mathbf{U}}_{\mathcal{J}}(\tilde{t}) \exp(\tilde{s}\tilde{t})]$, where Res stands for the residual of the terms between square brackets and the sum is extended to all the poles of $\tilde{\mathbf{U}}_{\mathcal{J}}(\tilde{t})$ (see also [60]). It may be worth remarking that the order of the inverse integral transforms can be exchanged by virtue of the Fubini theorem.

### *5.1. Compliance matrix*

In order to determine and discuss the forced response of the viscoelastic metamaterial, the dynamic compliance matrix $\mathbf{D}(\mathbf{b}, \tilde{s})$ can be analyzed first. To this purpose, the significant complex-valued components $D_{11}(\mathbf{b}, \tilde{s})$ and $D_{22}(\mathbf{b}, \tilde{s})$ are analyzed in the complex variable $\tilde{s}$-domain for a fixed nondimensional wavevector $\mathbf{b}$. Selecting the particular wavevector $\mathbf{b}_* = (1/3\pi\ 0)^\top$, the magnitudes of the components $D_{11}(\mathbf{b}, \tilde{s})$ and

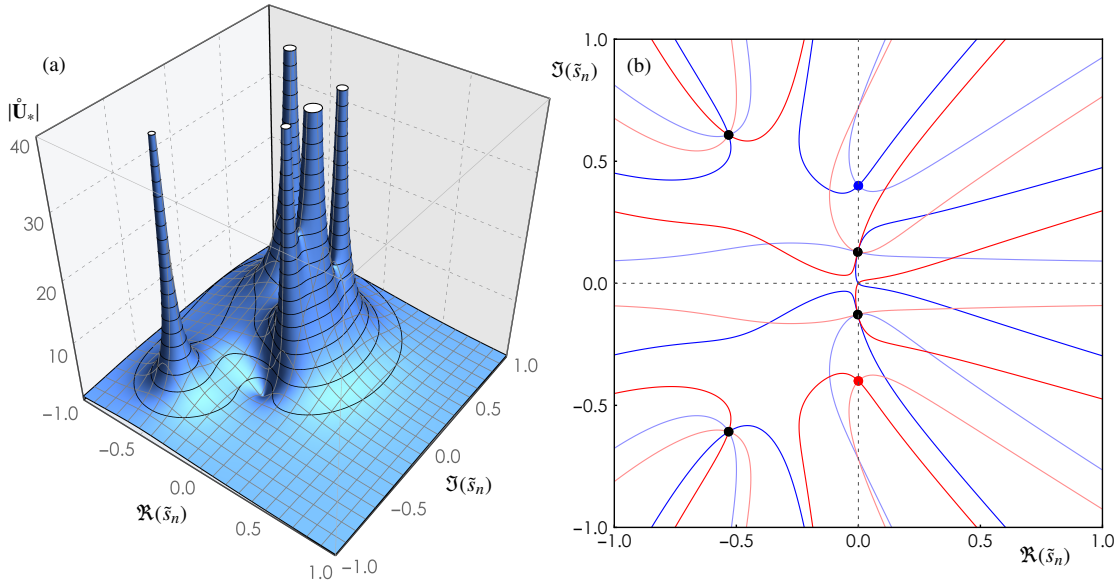


Figure 6: Forced response of the damped metamaterial $\mathcal{M}_d$ for fixed wavevector $\mathbf{b}_*$ in non-resonance conditions: (a) magnitude of the response $|\mathring{\mathbf{U}}|$ in the space of complex frequencies, (b) singularity points of the response $|\mathring{\mathbf{U}}|$ in the space of complex frequencies.

$D_{22}(\mathbf{b}, \tilde{s})$ are illustrated in Figures 5a and 5b for the particular metamaterial $\mathcal{M}_d$. The magnitude $|D_{11}|$ is characterized by rapidly but continuously growing values in the closeness of five well-distinct *poles at infinity* (Figures 5a). Similarly, the magnitude $|D_{22}|$ is characterized by rapidly but continuously growing values in the closeness of five poles at infinity, two of them practically unresolvable due to their proximity (Figures 5b). It is worth noting that the magnitudes of the two compliance matrix components do not possess common poles. In order to deepen the discussion, the continuous loci of the null real and null imaginary parts of the $|D_{11}|$-denominator (blue-scale curves) and $|D_{22}|$-denominator (red-scale curves) are reported in Figure 5c,d,e. The singularity points corresponding to the poles at infinity of the functions $|D_{11}|$ and $|D_{22}|$ can be detected as intersections of the blue-scale curves (blue dots) and intersections of the red-scale curves (red dots), respectively. For the sake of mathematical consistency, it is worth remarking that some intersections must be discarded from the set of singularities due to the coincidence between the identified zeros of the denominators and the zeros of the respective numerators (gray dots). As expected, the singularities occur either at pairs of complex-valued conjugate points (Figure 5c,d) or at single real-valued points (Figure 5e). The high resolution of Figure 5d allows also to distinguish the complex conjugate singularity points associated to the unresolved poles at infinity of Figure 5b. It can be verified that the discarded singularities (gray dots) actually identify poles at infinity of other matrix components, so that the entire set of singularity points (blue, red and gray dots) definitely mark all the poles of compliance matrix. Consequently, the singularity points also correspond to the complex-valued spectral components of the metamaterial for the fixed wavevector, including the components belonging to the weak-attenuation branches (Figure 5d) and pure-attenuation branches (Figure 5e).

### *5.2. Harmonic point force*

By virtue of the dynamic problem linearity and without loss of generality, it may be convenient to analyze the forced response to a single punctual excitation $\tilde{\mathbf{F}}_{\mathcal{J}}$ applied to the $\mathcal{J}$-th lattice node, taken as reference for the sake of simplicity (namely $\mathcal{J} = O$). Specifically, the generic mono-harmonic component $\tilde{\mathbf{F}}_O(\tilde{t}) = \tilde{\mathbf{F}}_{(0,\dots,0)}(\tilde{t}) = \eta^3 \tilde{\mathbf{P}} H(\tilde{t}) \exp(\tilde{S}\tilde{t})$ of a time-periodic force is considered, with constant amplitude $\eta^3\tilde{\mathbf{P}}$, complex nondimensional excitation frequency $\tilde{S}$ and $H(\tilde{t})$ indicating the unit step function. In particular, the analyses in the following are limited to non-decaying ($\Re(\tilde{S}) = 0$) or exponentially decaying ($\Re(\tilde{S}) < 0$) forces $\tilde{\mathbf{F}}_O$. Under these assumptions, the bilateral Laplace transform can be applied and, by virtue of relation (12), the

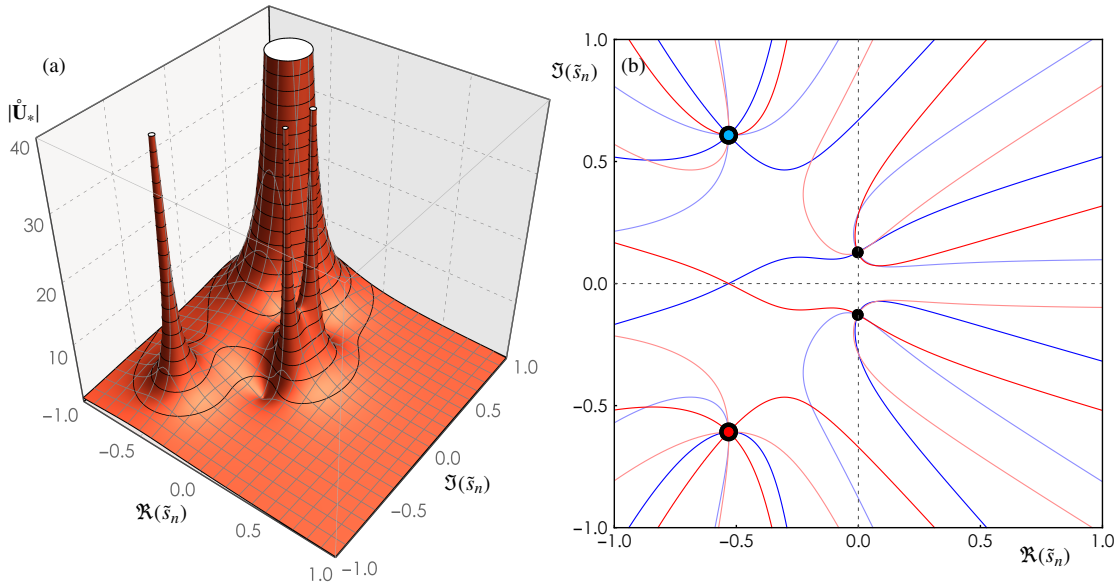


Figure 7: Forced response of the damped metamaterial $\mathcal{M}_d$ for fixed wavevector $\mathbf{b}_*$ in resonance conditions: (a) magnitude of the response $|\mathring{\mathbf{U}}|$ in the space of complex frequencies, (b) singularity points of the response $|\mathring{\mathbf{U}}|$ in the space of complex frequencies.

forcing term is independent of $\mathbf{z}$ (and then of $\mathbf{b}$), yielding

$$\mathring{\mathbf{F}}(\tilde{s}) = \hat{\mathbf{F}}(\tilde{s}) = \frac{\eta^3 \tilde{\mathbf{P}}}{\tilde{s} - \tilde{S}}, \tag{32}$$

where $\tilde{s} = \tilde{S}$ can be easily recognized as a singularity point in the complex variable $\tilde{s}$-domain, corresponding to a pole at infinity of the transformed external force. Null values are assigned to all the components of the amplitude $\tilde{\mathbf{P}}$, except the first component $\tilde{P}_1$ that is assumed unitary. From the algorithmic viewpoint, the forced response $\mathring{\mathbf{U}}(\mathbf{b}, \tilde{s})$ is initially obtained by employing equation (28). Subsequently, the actual possibility to exchange the orders of inverse transforms is exploited to determine the time-dependent response $\mathcal{L}^{-1}[\mathring{\mathbf{U}}(\mathbf{b}, \tilde{s})] = \check{\mathbf{U}}(\mathbf{b}, \tilde{t})$ first. Finally, the displacement $\tilde{\mathbf{U}}_O(\tilde{t})$ is determined for selected $\mathbf{b}$-values, in order to isolate significant contributions in the $\mathcal{B}$-domain to the time-dependent response.

The forced response of the prototypical damped metamaterial $\mathcal{M}_d$ is analyzed under two different key conditions of external excitation. The first is given by a non-decaying harmonic force with purely imaginary excitation frequency $\tilde{S}_s$ (exemplified by assigning the particular value $\tilde{S}/\eta = 4/10\imath$), while the second is given by an exponentially decaying harmonic force with complex excitation frequency $\tilde{S}_r$ (exemplified by assigning the particular value $\tilde{S}/\eta = \tilde{s}_*/\eta \simeq -12067/22701 + 6122/10073\imath$). The first excitation realizes a *non-resonance* condition, since the excitation frequency $\tilde{S}_s$ falls within the band gap separating the three low-frequency dispersion curves from the three high-frequency dispersion curves of the metamaterial spectrum. The second excitation realizes instead a *resonance* condition, since the excitation frequency $\tilde{S}_r$ is almost perfectly identical to the complex frequency $\tilde{s}_*$ belonging to the metamaterial spectrum at the particular wavevector $\mathbf{b}_*$. Considering first the non-resonance condition, the magnitude of the complex-valued response $\mathring{\mathbf{U}}_* = \mathring{\mathbf{U}}(\mathbf{b}_*, \tilde{s})$ varying in the complex variable $\tilde{s}$-domain is illustrated in Figure 6a. As expected, the magnitude $|\mathring{\mathbf{U}}_*| = \eta^3 |D_{11}/(\tilde{s} - \tilde{S}_s)|$ is characterized by rapidly but continuously growing values in the closeness of the same well-distinct poles at infinity already observed in the compliance component magnitude $|D_{11}|$ (Figures 6a). As major qualitative difference, an additional pole at infinity grows up around the $\tilde{S}_s$-value of the non-resonant excitation frequency. All the singularity points associated to the poles at infinity are distinguishable in the complex variable $\tilde{s}$-domain though the intersection of the blue-scale curves (Figure 6b), corresponding to the zeros of the $|\mathring{\mathbf{U}}_*|$-denominator. In particular, black dots indicate the singularity points of the compliance component magnitude $|D_{11}|$, while the blue dot indicates the additional singularity point of the external force. Finally, the intersections of the red-scaled curves correspond

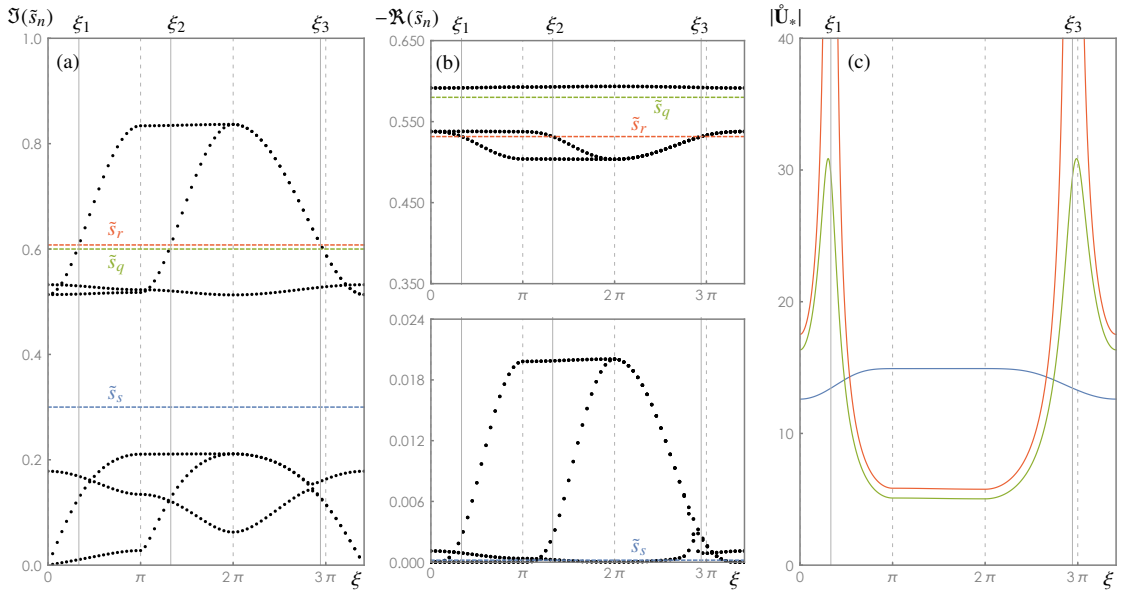


Figure 8: Forced response of the damped metamaterial $\mathcal{M}_d$ versus the wavevector for fixed non-resonant forcing frequency: (a),(b) selected complex variables $\tilde{s}_s$,$\tilde{s}_q$,$\tilde{s}_r$ in the imaginary and real parts of the dispersion spectrum, (c) magnitude of the forced response $\mathring{\mathbf{U}}(\xi, \tilde{s})$ versus the curvilinear abscissa $\xi$.

to the zeros of the $|\mathring{\mathbf{U}}_*|$-denominator when a complex-conjugate forcing frequency is employed. Accordingly, the red dot indicates the additional singularity point that complex conjugates the singularity point marked by the blue dot. Moving to consider the resonance condition, the magnitude $|\mathring{\mathbf{U}}_*| = \eta^3 |D_{11}/(\tilde{s} - \tilde{S}_r)|$ of the complex-valued response is illustrated in Figure 7a. Again, the magnitude $|\mathring{\mathbf{U}}_*|$ is characterized by the same well-distinct poles at infinity already observed in the compliance component magnitude $|D_{11}|$. As major qualitative difference, one of the pole at infinity dominates over the others. Looking at the singularity points in the complex variable $\tilde{s}$-domain (Figure 7b), it can be recognized that the dominant pole actually corresponds to a singularity point with double multiplicity, since the singularity point of the external force (blue dot) coalesces with one of the singularity points (black dots) of the compliance component.

In order to complete the discussion of the forced response $\mathring{\mathbf{U}}(\mathbf{b}, \tilde{s})$, the complementary case of fixed complex variable $\tilde{s}$ and varying wavevector $\mathbf{b}$ has to be considered for fixed forcing frequency $\tilde{S}_s$. Three different values of the complex variable $\tilde{s}$ are selected, as illustrated in Figure 8a,b. The first is a purely imaginary value $\tilde{s}_s$ (exemplified by assigning the particular value $\tilde{s}/\eta = 1/10\imath$), falling within the band gap separating the three low-frequency dispersion curves from the three high-frequency dispersion curves of the metamaterial spectrum (dashed blue lines). The second is a complex value $\tilde{s}_q$ (exemplified by assigning the particular value $\tilde{s}/\eta = -58/100 + 6/10\imath$) falling within the pass band of the high-frequency dispersion curves (dashed green lines). The third is a complex value $\tilde{s}_r$ (exemplified by assigning the particular value $\tilde{s}_*/\eta$) falling within the pass band, but also intersecting the high-frequency dispersion curves (dashed red lines). The intersections occur for different wavevectors, corresponding to particular values of the curvilinear abscissa $\xi$ spanning the closed boundary $\partial\mathcal{B}$ (specifically $\xi_1 = 1/3\pi$, $\xi_2 \simeq 31052/23419\pi$ and $\xi_3 \simeq 147811/50184\pi$). For each $\tilde{s}$-case, the magnitude of the forced response $\mathring{\mathbf{U}}(\xi, \tilde{s})$ is illustrated in Figure 8c. The magnitude associated to the purely imaginary value $\tilde{s}_s$ does not possess peaks neither poles at infinity (solid blue curve), as generally expected for all the complex $\tilde{s}$-values falling far away from the dispersion branches of the metamaterial spectrum. On the contrary, the magnitude associated to the complex value $\tilde{s}_r$ presents two poles at infinity corresponding to the intersection abscissae $\xi_1$ and $\xi_3$, as expected for all the complex $\tilde{s}$-values resonating with the dispersion branches at a certain $\xi$-value. The absence of a third pole at infinity corresponding to the intersection abscissae $\xi_2$ can be attributed to the orthogonality between the particular force vector $\tilde{\mathbf{P}}$ and the polarization vector at $\tilde{s}(\xi_2) = \tilde{s}_r$ for

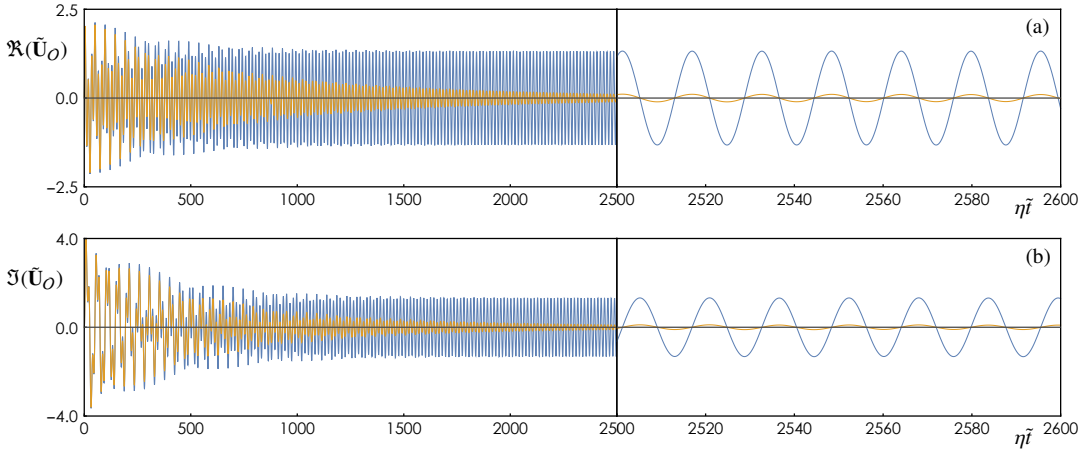


Figure 9: Time history of the complex-valued contribution at $\xi = 1/3\pi$ to the forced response of the metamaterial $\mathcal{M}_d$ for decaying and non-decaying external excitation: (a), real part (b) imaginary part.

the intersected dispersion branch. Finally, the magnitude associated to the complex value $\tilde{s}_q$ presents two sharp peaks in the proximity of the intersection abscissae $\xi_1$ and $\xi_3$, as expected for all the complex $\tilde{s}$-values quasi-resonating with the dispersion branches.

Significant contributions to the time-dependent response displacement $\tilde{\mathbf{U}}_O(\tilde{t})$ are determined for a selected pair of $\mathbf{b}$-values in the $\mathcal{B}$-domain (corresponding to $\xi = 1/3\pi$ and $\xi = \pi$). The time-histories of the real and imaginary parts of the function $\tilde{\mathbf{U}}_O(\tilde{t})$ are reported in Figures 9 and 10. For each $\mathbf{b}$-value, two different time-histories are compared, corresponding to a non-decaying harmonic external force (with purely imaginary frequency $\tilde{S}/\eta = 4/10\imath$) and a slightly-decaying harmonically external force (with complex frequency $\tilde{S}/\eta = -1/1000 + 4/10\imath$), respectively. The comparison shows that – after a certain transient – the stationary damped response to the non-decaying external force (blue time histories) oscillates with constant amplitude at the frequency of the external force, as expected. On the contrary, the damped response to the decaying external force (yellow time histories) oscillates with exponentially decreasing amplitudes. After the initial transient, the real and imaginary parts of the complex valued response to the non-decaying harmonic external force show no significant differences in the amplitudes, while their respective phases are in quadrature. Comparing the responses at different $\mathbf{b}$-values, they present similar contributions in the stationary amplitude, although the response at lower wavelengths ($\xi = \pi$) exhibit a shorter transient.

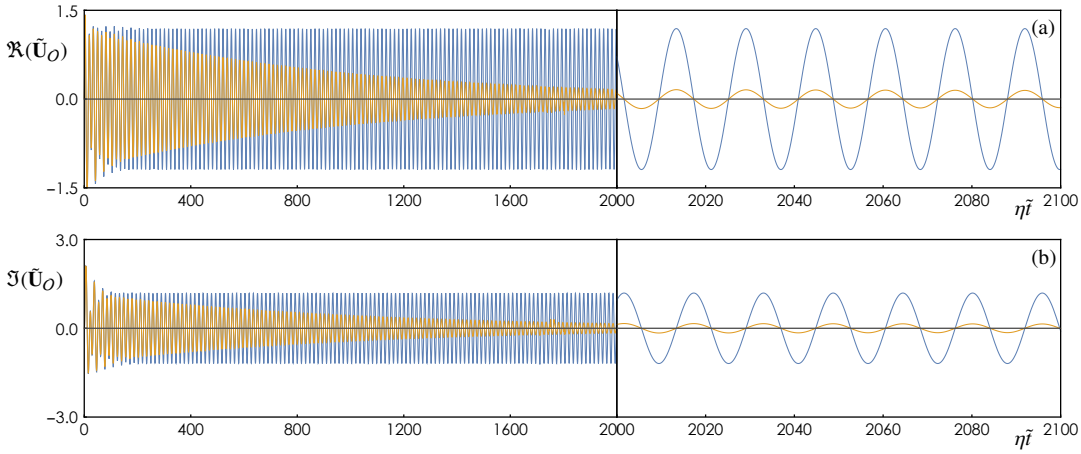


Figure 10: Time history of the complex-valued contribution at $\xi = \pi$ to the forced response of the metamaterial $\mathcal{M}_d$ for decaying and non-decaying external excitation: (a), real part (b) imaginary part.

## Conclusions

A general mechanical formulation has been presented for describing the linear wave dynamics of beam lattice materials, characterized by a periodic cellular microstructure composed by a geometrically repetitive pattern of rigid massive rings interconnected by flexible massless ligaments. The non-dissipative microstructure of the beam lattice has been enriched by introducing auxiliary damped oscillators, housed by the periodic rings and purposely tuned to realize a mechanical (or acoustic) metamaterial by exploiting the dynamic effect of local resonance. Each auxiliary oscillator, or resonator, has been viscoelastically coupled with the hosting ring. As peculiar aspect, the viscoelastic ring-resonator coupling has been derived by a proper mathematical formulation based on the Boltzmann superposition integral, whose kernel has been expressed by a Prony series. Accordingly, the free damped dynamics of the periodic cell is governed by a linear homogeneous system of integro-differential equations of motion. Therefore, imposing the quasi-periodicity conditions according to the Floquet-Bloch theory and applying the in-space $\mathcal{Z}$-transform and in-time bilateral Laplace transform, a linear coupled system of ordinary differential equations with frequency-dependent coefficients has been ascertained to govern the free damped wave propagation. Consequently, the associated nonlinear, non-polynomial eigenproblem has been stated. Two different solving strategies, based on either the eigenproblem de-rationalization or the eigenproblem approximation in power series of the Laplace variable, have been adopted to determine the complex-valued dispersion spectrum of the viscoelastic metamaterial.

Focusing on the metamaterial characterized by a quadrilateral periodic cell, the acoustic and optical branches of the complex-valued dispersion spectrum along the triangular boundary of the first Brillouin zone, spanned by real-valued wavenumbers, have been analyzed. Particularly, the complex spectra corresponding to different Laurent series approximations of the frequency-dependent rational coefficients governing the eigenproblem have been investigated, and the convergence has been successfully verified. The mathematical admissibility of certain eigensolutions has been discussed with reference to the boundaries limiting the convergence region of the Laurent series. The classic eigenproblem and the complex spectrum associated to the standard dynamic equations with linear viscous damping (Kelvin-Voigt viscoelastic coupling) have been recovered at the first-order approximation. Due to the non-polynomial nature of the eigenproblem coefficients, the exact eigensolution is characterized by a number of complex spectral branches that may exceed the model dimension. Exceeding spectral branches characterize also the convergent eigensolution for high-order approximations of the eigenproblem coefficients. From a qualitative viewpoint, the exceeding branches have been found to characterize the purely real-valued part of the complex spectrum, corresponding to standing waves that do not propagate in space but are damped in time. Focusing on the propagating waves, the exact and approximate eigensolutions shows that low-order approximations may determine non-negligible spectral effects in the high-frequency, strongly-attenuated, resonator-polarized branches of the spectrum. From a quantitative viewpoint, these spectral effects may also cause slight under-estimation of the stop bandwidth separating the low-frequency, weakly-attenuated branches from the high-frequency, strongly-attenuated branches.

Finally, the forced dynamics of the viscoelastic metamaterial under the effects of harmonically decaying and non-decaying excitations, given by an external mono-frequent point force acting on the microstructure, has been investigated. The metamaterial response has been determined and parametrically analyzed in terms of dynamic compliance matrices and displacement components, both in the frequency and the time domains. In particular, the existence of poles at infinity dominating the response functions, corresponding to singularity points in the Laplace domain, has been discussed and interpreted on the light of the metamaterial spectrum. Non-resonant, quasi-resonant and resonant conditions have been recognized, under the assumption of non-orthogonality between the force vector and the polarization eigenvector.

## Acknowledgments

The authors gratefully acknowledge the financial support of the (MIUR) Italian Ministry of Education, University and Research in the framework of the research MIUR Prin15 project 2015LYYXA8, "Multi-scale mechanical models for the design and optimization of micro-structured smart materials and metamaterials". The authors also acknowledge financial support by National Group of Mathematical Physics (GNFM-INdAM) and from the Compagnia San Paolo, project MINIERA no. I34I20000380007.

## AppendixA. Eigenproblem de-rationalization

The rational eigenvalue problem (20) can be de-rationalized in an equivalent quadratic form. Indeed, the eigenvalue problem can be first written in the convenient form

$$\left(\tilde{s}^2\mathbf{M} + \mathbf{S}(\tilde{s})\,(\tilde{s}\mathbf{G}_1 + \mathbf{G}_0) + \mathbf{H}\right)\mathring{\mathbf{U}}(\tilde{s}) = \mathbf{0}, \tag{A.1}$$

where the auxiliary matrices

$$\mathbf{S}(\tilde{s}) = \frac{\eta^2\tilde{t}_r}{\eta + \tilde{s}\tilde{t}_r}\mathbf{I}, \qquad \mathbf{S}^{-1}(\tilde{s}) = \frac{1}{\eta\tilde{t}_r}\mathbf{I} + \frac{\tilde{s}}{\eta^2}\mathbf{I} = \mathbf{R}_0 + \tilde{s}\,\mathbf{R}_1, \tag{A.2}$$

where the auxiliary matrices $\mathbf{R}_0$ and $\mathbf{R}_1$ have been introduced. Therefore the eigenvalue problem (A.1) can be expressed as

$$\left(\tilde{s}^2\mathbf{M} + \mathbf{H}\right)\mathring{\mathbf{U}}(\tilde{s}) + \mathring{\mathbf{Q}}(\tilde{s}) = \mathbf{0}, \tag{A.3}$$

where, under the condition $\tilde{s} \neq -\eta/\tilde{t}_r$ (corresponding to vanishing $\mathbf{S}^{-1}(\tilde{s})$), the auxiliary unknown

$$\mathring{\mathbf{Q}}(\tilde{s}) = \mathbf{S}(\tilde{s})\,(\tilde{s}\mathbf{G}_1 + \mathbf{G}_0)\,\mathring{\mathbf{U}}(\tilde{s}) = (\mathbf{R}_0 + \tilde{s}\,\mathbf{R}_1)^{-1}\,(\tilde{s}\mathbf{G}_1 + \mathbf{G}_0)\,\mathring{\mathbf{U}}(\tilde{s}). \tag{A.4}$$

Finally, the equation (A.3) and the relation (A.4) can be joined to state the equivalent eigenvalue problem

$$\begin{bmatrix} \tilde{s}^2\mathbf{M} + \mathbf{H} & \mathbf{I} \\ \tilde{s}\mathbf{G}_1 + \mathbf{G}_0 & -(\mathbf{R}_0 + \tilde{s}\,\mathbf{R}_1) \end{bmatrix}\begin{pmatrix} \mathring{\mathbf{U}}(\tilde{s}) \\ \mathring{\mathbf{Q}}(\tilde{s}) \end{pmatrix} = \begin{pmatrix} \mathbf{0} \\ \mathbf{0} \end{pmatrix}, \tag{A.5}$$

which can be reformulated as $\mathbf{L}(\tilde{s})\mathring{\mathbf{V}}(\tilde{s}) = \mathbf{0}$, where $\mathring{\mathbf{V}}(\tilde{s}) = (\mathring{\mathbf{U}}(\tilde{s})\;\mathring{\mathbf{Q}}(\tilde{s}))^\top$ and the quadratic matrix $\mathbf{L}(\tilde{s})$ can be written as

$$\mathbf{L}(\tilde{s}) = \tilde{s}^2\begin{bmatrix} \mathbf{M} & \mathbf{0} \\ \mathbf{0} & \mathbf{0} \end{bmatrix} + \tilde{s}\begin{bmatrix} \mathbf{0} & \mathbf{0} \\ \mathbf{G}_1 & -\mathbf{R}_1 \end{bmatrix} + \begin{bmatrix} \mathbf{H} & \mathbf{I} \\ \mathbf{G}_0 & -\mathbf{R}_0 \end{bmatrix}, \tag{A.6}$$

where the matrix coefficients of the $\tilde{s}$-unknown are singular by construction. Therefore, the quadratic eigenvalue problem $\mathbf{L}(\tilde{s})\mathring{\mathbf{V}}(\tilde{s}) = \mathbf{0}$ can be linearized according to AppendixB, if necessary.

## AppendixB. Eigenproblem linearization

The eigenvalue problem (23) can be expressed in an equivalent linear form $\mathbf{L}(\tilde{s})\mathring{\mathbf{V}}(\tilde{s}) = \mathbf{0}$, where $\mathring{\mathbf{V}}(\tilde{s}) = (\tilde{s}^{h-1}\mathring{\mathbf{U}}(\tilde{s}) \;\cdots\; \tilde{s}\mathring{\mathbf{U}}(\tilde{s})\;\mathring{\mathbf{U}}(\tilde{s}))^\top$ and the matrix $\mathbf{L}(\tilde{s})$ can be written as

$$\mathbf{L}(\tilde{s}) = \tilde{s}\begin{bmatrix} \mathbf{C}_h & \mathbf{0} & \cdots & \cdots & \cdots & \mathbf{0} \\ \mathbf{0} & \mathbf{I} & \ddots & \cdots & \cdots & \vdots \\ \vdots & \ddots & \ddots & \ddots & \cdots & \vdots \\ \vdots & \cdots & \ddots & \ddots & \ddots & \vdots \\ \vdots & \cdots & \cdots & \ddots & \ddots & \mathbf{0} \\ \mathbf{0} & \cdots & \cdots & \cdots & \mathbf{0} & \mathbf{I} \end{bmatrix} + \begin{bmatrix} \mathbf{C}_{h-1} & \mathbf{C}_{h-2} & \cdots & \mathbf{C}_j & \cdots & \mathbf{C}_0 \\ -\mathbf{I} & \mathbf{0} & \cdots & \cdots & \cdots & \mathbf{0} \\ \mathbf{0} & \ddots & \ddots & \cdots & \cdots & \vdots \\ \vdots & \ddots & \ddots & \ddots & \cdots & \vdots \\ \vdots & \cdots & \ddots & \ddots & \ddots & \vdots \\ \mathbf{0} & \cdots & \cdots & \mathbf{0} & -\mathbf{I} & \mathbf{0} \end{bmatrix}. \tag{B.1}$$

Consequently, the eigenvalues solving the eigenvalue problem (23) coincide with the $\tilde{s}$-values that make the auxiliary higher-dimensional matrix $\mathbf{L}(\tilde{s})$ singular. The corresponding eigenvectors $\mathring{\mathbf{U}}(\tilde{s})$ coincide with a subvector of the vector $\mathring{\mathbf{V}}(\tilde{s})$.

## References


[1] N. Fleck, V. Deshpande, M. Ashby, Micro-architectured materials: past, present and future, Proceedings of the Royal Society of London A: Mathematical, Physical and Engineering Sciences 466 (2121) (2010) 2495–2516.

[2] L. R. Meza, A. J. Zelhofer, N. Clarke, A. J. Mateos, D. M. Kochmann, J. R. Greer, Resilient 3d hierarchical architected metamaterials, Proceedings of the National Academy of Sciences 112 (37) (2015) 11502–11507.

[3] T. A. Schaedler, W. B. Carter, Architected cellular materials, Annual Review of Materials Research 46 (2016) 187–210.

[4] M. Kadic, G. W. Milton, M. van Hecke, M. Wegener, 3d metamaterials, Nature Reviews Physics 1 (2019) 198–210.

[5] Y.-F. Wang, Y.-Z. Wang, B. Wu, W. Chen, Y.-S. Wang, Tunable and active phononic crystals and metamaterials, Applied Mechanics Reviews 72 (4) (2020) 040801.

[6] J.-H. Lee, J. P. Singer, E. L. Thomas, Micro-/nanostructured mechanical metamaterials, Advanced materials 24 (36) (2012) 4782–4810.

[7] M. Rashed, M. Ashraf, R. Mines, P. J. Hazell, Metallic microlattice materials: A current state of the art on manufacturing, mechanical properties and applications, Materials & Design 95 (2016) 518–533.

[8] Y. Sha, L. Jiani, C. Haoyu, R. O. Ritchie, X. Jun, Design and strengthening mechanisms in hierarchical architected materials processed using additive manufacturing, International Journal of Mechanical Sciences 149 (2018) 150–163.

[9] X. Zheng, H. Lee, T. H. Weisgraber, M. Shusteff, J. DeOtte, E. B. Duoss, J. D. Kuntz, M. M. Biener, Q. Ge, J. A. Jackson, S. O. Kucheyev, N. X. Fang, C. M. Spadaccini, Ultralight, ultrastiff mechanical metamaterials, Science 344 (6190) (2014) 1373–1377.

[10] J. T. Overvelde, J. C. Weaver, C. Hoberman, K. Bertoldi, Rational design of reconfigurable prismatic architected materials, Nature 541 (7637) (2017) 347–352.

[11] W. Wu, W. Hu, G. Qian, H. Liao, X. Xu, F. Berto, Mechanical design and multifunctional applications of chiral mechanical metamaterials: A review, Materials & Design (2019) 107950.

[12] H. Kolken, K. Lietaert, T. van der Sloten, B. Pouran, A. Meynen, G. Van Loock, H. Weinans, L. Scheys, A. A. Zadpoor, Mechanical performance of auxetic meta-biomaterials, Journal of the mechanical behavior of biomedical materials 104 (2020) 103658.

[13] M.-H. Lu, L. Feng, Y.-F. Chen, Phononic crystals and acoustic metamaterials, Materials today 12 (12) (2009) 34–42.

[14] M. I. Hussein, M. J. Leamy, M. Ruzzene, Dynamics of phononic materials and structures: Historical origins, recent progress, and future outlook, Applied Mechanics Reviews 66 (4) (2014) 040802.

[15] K. Bertoldi, V. Vitelli, J. Christensen, M. van Hecke, Flexible mechanical metamaterials, Nature Reviews Materials 2 (11) (2017) 17066.

[16] P. G. Malischewsky, A. Lorato, F. Scarpa, M. Ruzzene, Unusual behaviour of wave propagation in auxetic structures: P-waves on free surface and s-waves in chiral lattices with piezoelectrics, physica status solidi (b) 249 (7) (2012) 1339–1346.

[17] J. Dirrenberger, S. Forest, D. Jeulin, Effective elastic properties of auxetic microstructures: anisotropy and structural applications, International Journal of Mechanics and Materials in Design 9 (1) (2013) 21–33.

[18] B. Florijn, C. Coulais, M. van Hecke, Programmable mechanical metamaterials, Physical Review Letters 113 (17) (2014) 175503.

[19] D. J. Colquitt, M. Brun, M. Gei, A. Movchan, N. Movchan, I. Jones, Transformation elastodynamics and cloaking for flexural waves, Journal of the Mechanics and Physics of Solids 72 (2014) 131–143.

[20] J. Berger, H. Wadley, R. McMeeking, Mechanical metamaterials at the theoretical limit of isotropic elastic stiffness, Nature 543 (7646) (2017) 533–537.

[21] C. Coulais, D. Sounas, A. Alù, Static non-reciprocity in mechanical metamaterials, Nature 542 (7642) (2017) 461–464.

[22] A. Bacigalupo, M. Lepidi, Acoustic wave polarization and energy flow in periodic beam lattice materials, International Journal of Solids and Structures 147 (2018) 183–203.

[23] L. D'Alessandro, R. Ardito, F. Braghin, A. Corigliano, Low frequency 3D ultra-wide vibration attenuation via elastic metamaterial, Scientific Reports 9 (1) (2019) 8039.

[24] G. Bordiga, L. Cabras, D. Bigoni, A. Piccolroaz, Free and forced wave propagation in a Rayleigh-beam grid: flat

bands, Dirac cones, and vibration localization vs isotropization, International Journal of Solids and Structures 161 (2019) 64–81.

[25] F. Dal Corso, D. Tallarico, N. V. Movchan, A. B. Movchan, D. Bigoni, Nested Bloch waves in elastic structures with configurational forces, Philosophical Transactions of the Royal Society A 377 (2156) (2019) 20190101.

[26] Y. Chen, T. Li, F. Scarpa, L. Wang, Lattice metamaterials with mechanically tunable Poisson's ratio for vibration control, Physical Review Applied 7 (2) (2017) 024012.

[27] M. Lepidi, A. Bacigalupo, Parametric design of the band structure for lattice materials, Meccanica 53 (3) (2018) 613–628.

[28] H. Ronellenfitsch, N. Stoop, J. Yu, A. Forrow, J. Dunkel, Inverse design of discrete mechanical metamaterials, Physical Review Materials 3 (9) (2019) 095201.

[29] A. Bacigalupo, L. Gambarotta, Dispersive wave propagation in two-dimensional rigid periodic blocky materials with elastic interfaces, Journal of the Mechanics and Physics of Solids 102 (2017) 165–186.

[30] M. Lepidi, A. Bacigalupo, Multi-parametric sensitivity analysis of the band structure for tetrachiral acoustic metamaterials, International Journal of Solids and Structures 136-137 (2018) 186–202.

[31] M. C. Messner, Optimal lattice-structured materials, Journal of the Mechanics and Physics of Solids 96 (2016) 162–183.

[32] A. Bacigalupo, M. Lepidi, G. Gnecco, F. Vadalà, L. Gambarotta, Optimal design of the band structure for beam lattice metamaterials, Frontiers in Materials 6 (2019) 2.

[33] M. Bruggi, A. Corigliano, Optimal 2d auxetic micro-structures with band gap, Meccanica 54 (13) (2019) 2001–2027.

[34] A. Bacigalupo, G. Gnecco, M. Lepidi, L. Gambarotta, Machine-learning techniques for the optimal design of acoustic metamaterials, Journal of Optimization Theory and Applications doi:10.1007/s10957-019-01614-8.

[35] G. Ma, P. Sheng, Acoustic metamaterials: From local resonances to broad horizons, Science advances 2 (2) (2016) e1501595.

[36] I. V. Kamotski, V. P. Smyshlyaev, Bandgaps in two-dimensional high-contrast periodic elastic beam lattice materials, Journal of the Mechanics and Physics of Solids 123 (2019) 292–304.

[37] A. Krushynska, V. Kouznetsova, M. Geers, Towards optimal design of locally resonant acoustic metamaterials, Journal of the Mechanics and Physics of Solids 71 (2014) 179–196.

[38] A. Bacigalupo, M. Lepidi, High-frequency parametric approximation of the Floquet-Bloch spectrum for anti-tetrachiral materials, International Journal of Solids and Structures 97-98 (2016) 575–592.

[39] A. Casalotti, S. El-Borgi, W. Lacarbonara, Metamaterial beam with embedded nonlinear vibration absorbers, International Journal of Non-Linear Mechanics 98 (2018) 32–42.

[40] A. Bacigalupo, G. Gnecco, M. Lepidi, L. Gambarotta, Optimal design of low-frequency band gaps in anti-tetrachiral lattice meta-materials, Composites Part B 115 (2017) 341–359.

[41] F. Romeo, A. Luongo, Vibration reduction in piecewise bi-coupled periodic structures, Journal of Sound and Vibration 268 (3) (2003) 601–615.

[42] D. Bigoni, S. Guenneau, A. Movchan, M. Brun, Elastic metamaterials with inertial locally resonant structures: Application to lensing and localization, Physical Review B 87 (17) (2013) 174 303.

[43] M. Morvaridi, G. Carta, M. Brun, Platonic crystal with low-frequency locally-resonant spiral structures: wave trapping, transmission amplification, shielding and edge waves, Journal of the Mechanics and Physics of Solids 121 (2018) 496–516.

[44] L. Morini, Y. Eyzat, M. Gei, Negative refraction in quasicrystalline multilayered metamaterials, Journal of the Mechanics and Physics of Solids 124 (2019) 282–298.

[45] R. Lakes, Viscoelastic materials, Cambridge university press, 2009.

[46] M. I. Hussein, Theory of damped Bloch waves in elastic media, Physical Review B 80 (21) (2009) 212301.

[47] J. M. Manimala, C. Sun, Microstructural design studies for locally dissipative acoustic metamaterials, Journal of Applied Physics 115 (2) (2014) 023518.

[48] A. S. Phani, M. I. Hussein, Analysis of damped Bloch waves by the Rayleigh perturbation method, Journal of Vibration and Acoustics 135 (4) (2013) 041014.

[49] M. J. Frazier, M. I. Hussein, Viscous-to-viscoelastic transition in phononic crystal and metamaterial band structures, The Journal of the Acoustical Society of America 138 (5) (2015) 3169–3180.

[50] W. Drugan, Wave propagation in elastic and damped structures with stabilized negative-stiffness components,

Journal of the Mechanics and Physics of Solids 106 (2017) 34–45.

[51] F. Romeo, A. Paolone, Wave propagation in three-coupled periodic structures, Journal of Sound and Vibration 301 (3-5) (2007) 635–648.

[52] F. Farzbod, M. J. Leamy, Analysis of Bloch's method in structures with energy dissipation, Journal of Vibration and Acoustics 133 (5) (2011) 051010.

[53] R. P. Moiseyenko, V. Laude, Material loss influence on the complex band structure and group velocity in phononic crystals, Physical Review B 83 (6) (2011) 064301.

[54] E. Andreassen, J. S. Jensen, Analysis of phononic bandgap structures with dissipation, Journal of Vibration and Acoustics 135 (4) (2013) 041015.

[55] A. Krushynska, V. Kouznetsova, M. Geers, Visco-elastic effects on wave dispersion in three-phase acoustic metamaterials, Journal of the Mechanics and Physics of Solids 96 (2016) 29–47.

[56] M. Lewińska, V. Kouznetsova, J. van Dommelen, A. Krushynska, M. Geers, The attenuation performance of locally resonant acoustic metamaterials based on generalised viscoelastic modelling, International Journal of Solids and Structures 126 (2017) 163–174.

[57] M. V. Barnhart, X. Xu, Y. Chen, S. Zhang, J. Song, G. Huang, Experimental demonstration of a dissipative multi-resonator metamaterial for broadband elastic wave attenuation, Journal of Sound and Vibration 438 (2019) 1–12.

[58] J. D. Ferry, Viscoelastic properties of polymers, John Wiley & Sons, 1980.

[59] R. Christensen, Theory of viscoelasticity: an introduction, Elsevier, 2012.

[60] G. B. Arfken, H. J. Weber, F. E. Harris, Mathematical Methods for Physicists, Academic Press, 2013.

[61] Y. Su, Z. Bai, Solving rational eigenvalue problems via linearization, SIAM Journal on Matrix Analysis and Applications 32 (1) (2011) 201–216.